This project is part of the PRIMA Programme supported by the European Union

RESERVOIR

Sustainable groundwater RESources managEment by integrating eaRth observation deriVed monitoring and flOw modelIng Results

PRIMA

GA no. 1924

DELIVERABLE D5.4

Groundwater Flow Model for the Azraq Wetland Reserve (Jordan)

Author(s):	DEU: M. Berker Bayırtepe, Alper Elçi UJ: Alsharifa Hind Mohammad, Qamar Al-Mimi, Khaldoun Shatanawi
Responsible Partner:	DEU
Version:	Final
Date:	30 December 2022
Distribution Level (CO, PU)	PU

Acknowledgement

This project has received funding from the Partnership for Research and Innovation in the Mediterranean Area under the European Union's Horizon 2020 research and innovation programme under grant agreement No 1924.

Statement of Originality

This document contains original unpublished work except where clearly indicated otherwise. Acknowledgement of previously published material and of the work of others has been made through appropriate citation, quotation or both.

Disclaimer

This publication reflects the authors' views. The consortium is not responsible for any use that may be made of the information it contains. The information contained in this document and any other information linked therein is confidential, privileged and it remains the property of its respective owner(s). As such, and under the conditions settled in the RESERVOIR Grant Agreement and the RESERVOIR Consortium Agreement, it is disclosed for the information of the intended recipients within the RESERVOIR Consortium and the European Commission / PRIMA according to its "Dissemination Level"* and may not be used, published or redistributed without the prior written consent of its owner(s).

* PU = Public; CO = Confidential, only for members of the consortium EU-R/R-UE = Classified, as referred to in Commission Decision 2001/844/EC.

DOCUMENT REVISION HISTORY

Date	Version	Editor(s)	Comments	Status
15.12.2022	0.1	Alper Elçi (DEU), Berker Bayırtepe (DEU)		Draft
18.12.2022	0.1	Alsharifa Hind Mohammad (UJ), Qamar Al-Mimi (RSCN)	Added descriptions about groundwater recharge and pumping wells	Draft
27.12.2022	0.2	Alper Elçi (DEU), Berker Bayırtepe (DEU)	Distributed to the consortium for review	Draft
28.12.2022	0.2	Pietro Teatini (UNIPD)		Draft
29.12.2022	0.2	Khaldoun Shatanawi (UJ)		Draft
29.12.2022	0.2	A. Hakan Ören		Draft
30.12.2022	1.0	Alper Elçi (DEU)		Final
10.04.2023	1.1	Alper Elçi (DEU)	Improved some maps	Final

LIST OF PARTNERS

Participant	Name	Country
UNIPV	Università degli Studi di Pavia	Italy
UNIPD	Università di Padova	Italy
IGME	Instituto Geológico y Minero de España	Spain
UA	Universidad de Alicante	Spain
DEU	Dokuz Eylül University	Turkey
UJ	The University of Jordan	Jordan
CER	Consorzio di Bonifica di secondo grado per il Canale Emiliano Romagnolo	Italy
RSCN-AWR	Royal Society for the Conservation of Nature - Azraq Wetland Reserve	Jordan

GLOSSARY

Acronym	Description
AOI	Area of Interest
AWR	Azraq Wetland Reserve
DEM	Digital Elevation Model
GUI	Graphical User Interface
EO	Earth-Observation
ETP	Evapotranspiration
K	Hydraulic Conductivity
MAE	Mean Absolute Error
MWI	Ministry of Water and Irrigation
PWS	Public Water Supply
RMSE	Root Mean Squared Error
S	Storativity / Storage Coefficient
T	Transmissivity
WP	Work Package

CONTENTS

LIST OF FIGURES AND TABLES

1. INTRODUCTION

1.1 Goal and Purpose of this Document

The RESERVOIR project aims to provide new products and services for a sustainable groundwater management model to be developed and tested in four water-stressed Mediterranean pilot sites and then be applicable in other regions via an interdisciplinary approach.

The specific Project Objectives (PO) are the following:

- PO1. Develop an innovative methodology for the hydrogeological characterization of large-scale aquifer systems using low-cost and non-intrusive data such as satellite-based Earth Observation (EO) techniques.
- PO2. Integrate advanced EO techniques into numerical groundwater flow and geomechanical models to improve the knowledge about the current capacity to store water and the future response of aquifer systems to natural and human-induced stresses.
- PO3. Enhance the knowledge about the impacts of agricultural and tourism activities on the water resources by quantifying the ground deformation during the monitored periods.
- PO4. Engage water management authorities and provide models for optimal management of the aquifer systems. We will engage 4 water authorities in 4 different countries through a series of face-to-face workshops (each participant will organize at least 1 workshop in the first 4 months of the project). The water authorities will be involved in the conceptualization and design of guidelines for Groundwater Resource Management (GRM). Best practices of water management for agricultural and tourism purposes will be developed taking advantage of the knowledge and methodologies from the outputs of PO1, PO2, and PO3.
- PO5. Dissemination and exchange of the generated knowledge among the experts and the managers in charge of land and groundwater management in the pilot sites to strengthen the aquifer resilience.

The main objective of WP5 is to develop groundwater flow models for all pilot sites. The models are calibrated against time series of historical hydraulic head measurements and the calibrated models are subsequently used to simulate groundwater flow for the analyzed period of EO data, i.e. processed A-DInSAR observation period. Through the integration of EO observations into these numerical groundwater flow models, the current capacity to store water and the future response of the aquifer to climate and global change-related stresses are simulated.

WP5 is subdivided into five tasks, corresponding to the groundwater flow models of each pilot site and an additional task (T5.5) that involves the implementation of the integration of D-InSAR with the flow models:

- T5.1 – Development, calibration, and application of the variable-density groundwater flow model for the coastal aquifer of Comacchio (Italy)
- T5.2 – Development, calibration, and application of the groundwater flow model for the Alto Guadalentín aquifer (Spain)
- T5.3 – Development, calibration, and application of the groundwater flow model for the alluvial aquifer of Gediz River Basin (Turkiye)

- T5.4 – Development, calibration, and application of the groundwater flow model for the Azraq Wetland Reserve (Jordan)
- T5.5 – Simulation results for the EO data-optimized GW flow models

In this deliverable, a detailed technical report of Task 5.4, the groundwater flow model for the Jordan pilot site, the Azraq Wetland Reserve (AWR) is presented. A regional, three-dimensional transient groundwater flow model is developed for the Azraq watershed using Modelmuse version 5.1.1 (Winston, 2022), which is a public-domain GUI of the finite-difference flow model MODFLOW (Harbaugh et al., 2019).

1.2 Modeling Objectives

The specific objectives of this modeling study and the intended uses include the following:

1) To simulate changes in groundwater storage that can be subsequently related to land subsidence with a coupled geomechanical model;
2) To develop a mathematical model that advances understanding of the groundwater flow dynamics in and around the Azraq Wetland Reserve area;
3) To provide a tool that supports the management of groundwater intending to preserve the groundwater-dependent wetland ecosystem;
4) To determine critical areas of decline in groundwater levels;
5) To develop a mathematical model that enables the analysis of groundwater budgets;
6) To develop a mathematical model that can be further used to evaluate the impacts of climate change scenarios;

1.3 General Description of Model Area

The Azraq Basin is an extensive transboundary watershed in the northern part of the Eastern Desert of Jordan (Figure 1-1). It provides the largest resource of good-quality groundwater in the northeast of Jordan. The drainage area of the watershed is 12,414 km^2 that extends from the Syrian borders in the north to the Saudi Arabian borders in the south. About 94% of the Azraq Basin (Figure 1-2) is located within the political boundaries of Jordan and the remaining part is in Syria. Topographically, the basin is concave with the Azraq oasis as a large fertile mudflat in the central and lowest part of the basin.

The Azraq Basin is a major source of drinking water for the major cities in Jordan (Amman, Zarqa, and Irbid) and also for the Azraq region itself. The total groundwater abstraction from the basin in 2010 was about 53 Mm^3/yr while the safe abstraction limit is estimated as 24 Mm^3/yr. Agricultural activities are prevalent and are concentrated in the northern and western parts of the basin, also in the basin center near the town of Azraq. Intensive pumping over the last 20 years has caused a decline in the water table and, consequently, an increase in groundwater salinity.

The selected pilot site for the scope of the RESERVOIR project is the Azraq Wetland Reserve (AWR), also referred to as the Azraq oasis, which is located in the center of the Azraq Basin. It is designated as a RAMSAR site in Jordan according to the Convention on Wetlands. The oasis is important for migratory birds, and millions of birds can be seen in and around the wetland area during spring migration every year. However,

the oasis is under severe environmental stresses and the ecosystem is in a far stage of degradation. The main cause of the oasis deterioration is groundwater overexploitation in the basin beginning in the early 1980s. By the end of 1992, both springs within the AWR ceased to flow. Therefore, in 1994, an agreement between the government and the Royal Scientific Society for Nature Conservation was signed to pump groundwater from an MWI well located near Soda Spring to the surface of the oasis area. The water is distributed across the AWR by supplying water to the ponds, in particular to the Shishan pond, which helped conserve 10-15 % of the Shishan marches.

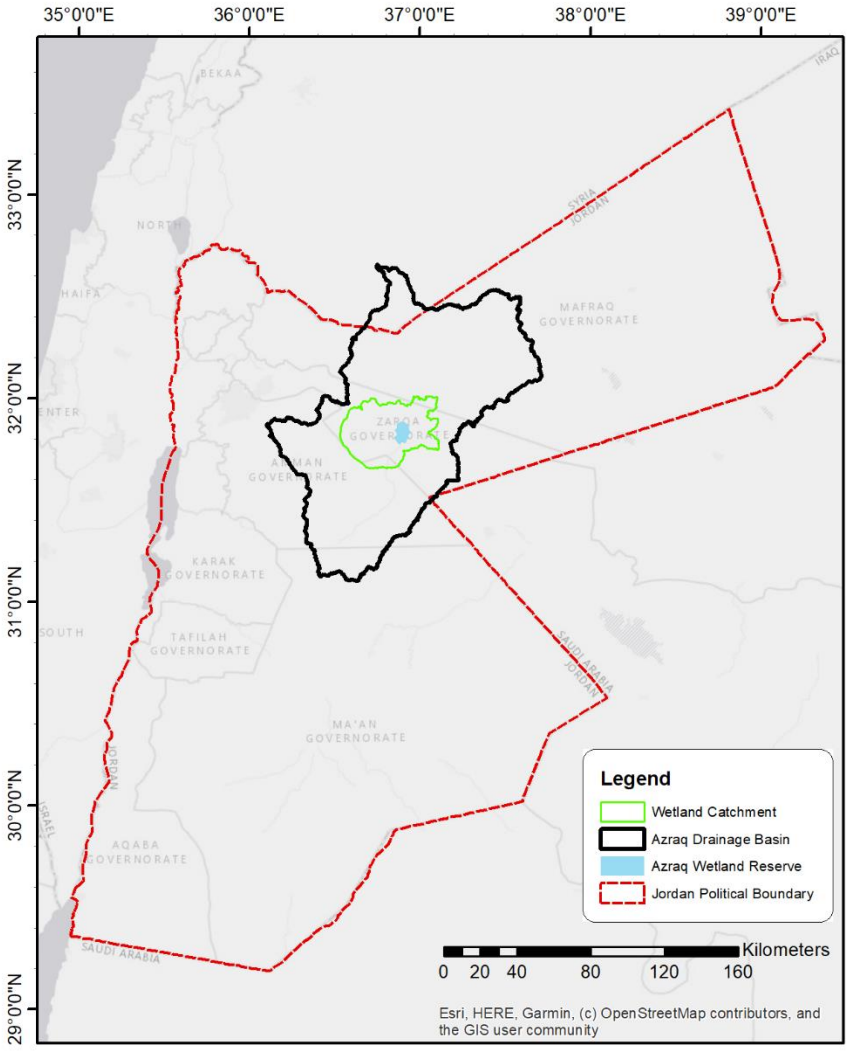

Figure 1-1. The geographic location of the Azraq Basin.

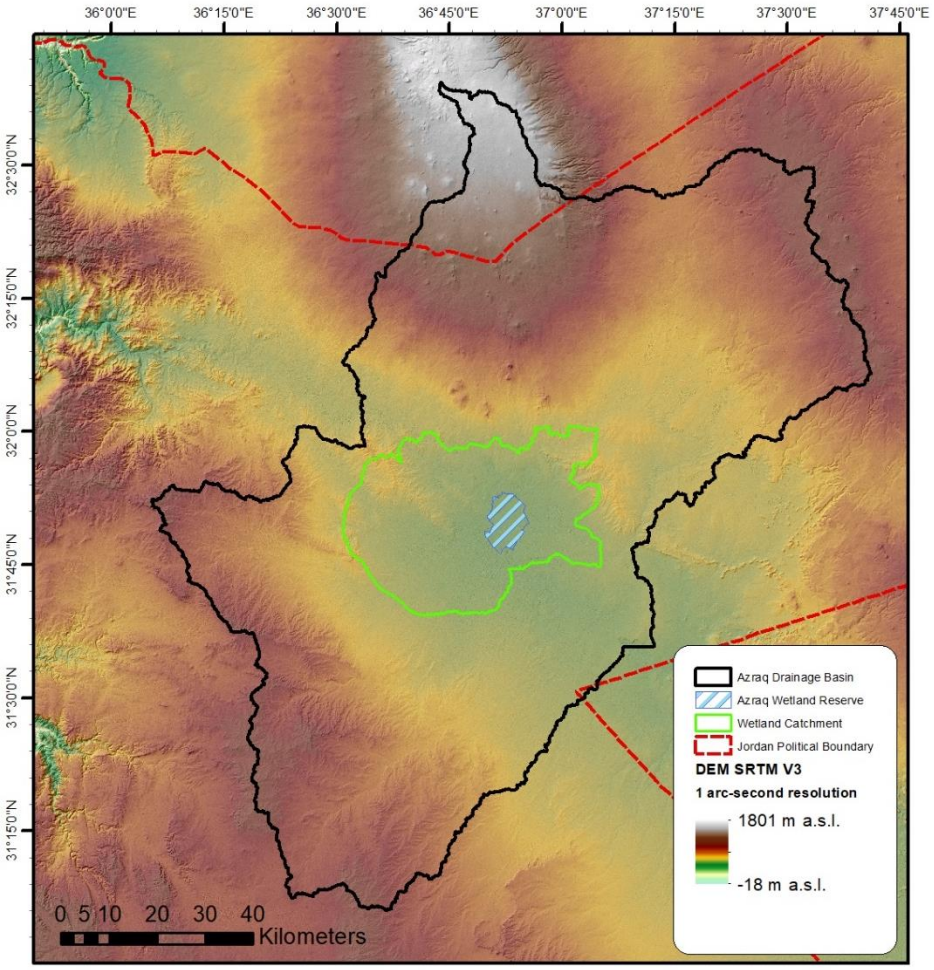

Figure 1-2. The layout of Azraq Basin, wetland catchment, and the Azraq Wetland Reserve.

1.3.1 Geological Setting

The Azraq Basin covers part of the limestone plateau in eastern Jordan. The north-eastern part of the basin is mainly covered by basaltic lava originating from Miocene/Oligocene volcanic activity. The basalt reaches a thickness of more than 1500 m in the area of Mount Arab in Syria and becomes progressively thinner towards the south. The area is characterized by two different domains, mainly composed of sedimentary rocks and basalts. In the southern part of the area and on the surface, Quaternary covers are located above Tertiary deposits. The latter are exposed locally at the surface in the southern part of the area. In the subsurface of this area, a thick sedimentary section (averagely higher than 3500 m), that is changing in thickness and varying in the lithostratigraphic and formation units, represents the basin. These sediments are primarily composed of carbonates, sandstones, and shales. The major thickness reduction in the sequence appears towards the south and southwest directions, while a remarkable increase in thickness is observed east of Azraq town towards the Fuluq fault, which limits the basin to the south and southeast directions. The lower Cretaceous boundary of this sequence is represented by a sandstone formation underlying the carbonate

facies of the Cenomanian age. This sandstone unit varies in thickness and depth and marks the transition zone on the major unconformity between the Jurassic and the early Cretaceous.

In the northern part of the area, basalt eruptions of different ages (from Tertiary to Quaternary) appear on the surface and extend northwards to cover a wide area known as the Basalt Plateau, which is related to the North Arabian Volcanic Province extending from Syria across Jordan into Saudi Arabia. Basaltic rocks are characterized by an age ranging from 26 to < 0.5 million years (Illani et al., 2001). In addition to the basaltic lava, which erupted from elongated fissures forming a flood basalt plateau, the volcanism also includes pyroclastic deposits (a stratified volcanic tuff formation and an ill-graded agglomeratic scoria formation), that resulted from point source volcanoes. The volcanic activity is interbedded and followed by the local deposition of clays, evaporites, sandstone, diatomite, and limestone. Azraq basin is tectonically active and dominated by NW-SE, E-W, NE-SW, and N-S faults and lineaments. NW-SE and the EW fault systems are the main ones believed to have controlled the development of the Azraq depression and the former Azraq Lake. The regional dip is located east-southeast of the AWR. Folds are relatively small with gentle dip and are mainly associated with some NW-SE faults and lineaments.

1.3.2 Climatic Setting

The climate of the Azraq Basin is characterized by two well-defined seasons, hot and dry summer, and relatively wet and cold winter. Ayed (1996) conducted a comprehensive study on the climatological and hydrological variables of the Azraq Basin. The record length extends from 1967 to 1995. Most of the study area is arid and a small portion can be considered semiarid. According to the Ayed (1996) study, the average relative humidity varied from 49.9 to 61% in summer and from 56 to 82% in winter. The average annual minimum and maximum temperatures are 11.6 °C and 26.6 °C, respectively. The coldest month of the year is January while the hottest months are July and August. The Azraq drainage basin is irregular in shape and forms a relatively shallow depression with a central playa (Qa'a Azraq), surrounded by mudflats and salt pans. The area is typical for arid to semiarid zones. The precipitation ranges from 50 mm/yr in Azraq Oasis to 500 mm/yr in Jabal Arab. The average precipitation for the entire basin is 87 mm/yr, most of which occurs as storms between January to March (El-Naqa, 2010). Annual rainfall patterns in the Jordanian part of the basin vary between 100-150 mm in the west and north of the basin, 50-100 mm in the center, and less than 50 mm in the south and east of the basin. The average evaporation rate in the area is 2,400 mm/yr.

Based on the records of the meteorological stations in the Azraq Basin the long-term annual precipitation ranges from 52 mm to 88 mm. On a monthly basis; December to April is the wettest time of the year, while no rainfall is recorded during the months of June to September. Minimum (average 3.1 °C) and maximum (average 36.8 °C) temperatures occur in January and August, respectively. Long-term averages of rainfall and temperature measurements recorded at a meteorological station in the Azraq Basin are shown in Figure 1-3.

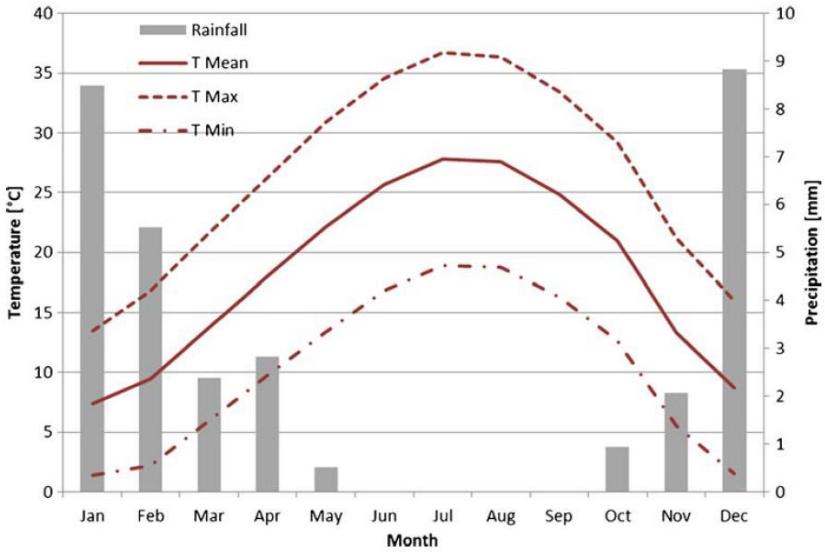

Figure 1-3. 10-year average of temperature and rainfall for Station F0009 near Azraq (Ibrahim and El-Naqa, 2018).

1.3.3 Hydrogeology

The aquifers in the basin are major sources of drinking water for the main cities in Jordan (Amman, Zarqa, and Irbid) as well as for the Azraq area itself. Figure 1-4 shows the hydrogeological units in the Azraq Basin. The Azraq Basin consists of three aquifer systems hydraulically connected in certain parts; upper, middle, and deeper aquifer systems. In particular, the upper aquifer is exposed in the entire basin and consists of four major water-bearing formations: B4, B5, the Basalt (Ba), and the Quaternary formation. The basalt extends from the center of the basin to the north and ends up in the highlands of Syria. Groundwater flows from south Syria towards Jordan from high to lower elevations (1,172 m a.s.l. to 492 m a.s.l.) towards the Azraq depression. The depth of groundwater in the upper aquifer varies from a few meters in the center of the Azraq oasis to 400 m due to the topography in the northern catchment area.

The Middle Aquifer System is known as Amman-Wadi Sir (A7/B2) Aquifer System. It is a confined aquifer due to the presence of bituminous marl of the (B3) formation. This aquifer system underlies the Upper Aquifer System and outcrop in the western part of the basin. The Amman Formation (B2-Aquifer) is composed of chert, chalk, and limestone. The (A7) formation of the second aquifer forms one composite aquifer system with the (B2) Formation. At least 38 wells penetrating the A7/B2 Aquifer System were drilled in the Azraq Basin. The A7/B2 aquifer composed of karstic limestone and chert formations is overlain by the B3 aquitard (confining) formation. The deeper aquifer system (A1/A6) is a unit between A7/B2 and the Kurnub Sandstone aquifer, which is characterized by low yield and poor water quality (saline aquifer).

Abstraction of water from the Azraq Basin by the government and local farmers increased dramatically from the early 1980s. As a result of groundwater over-exploitation in recent decades, groundwater levels declined significantly leading to the drying of springs in the early 1990s. Figure 1-5 shows groundwater levels at different wells located in the Azraq Basin. In addition, excessive abstraction has reduced groundwater levels in the wetland area. Prior to increased abstraction, the groundwater level within the AWR was close to the soil surface for most of the year. Since excessive pumping from the aquifer began, however, the groundwater table has been declining, and a present it lies around 20 m below the soil surface (IWMI, 2017).

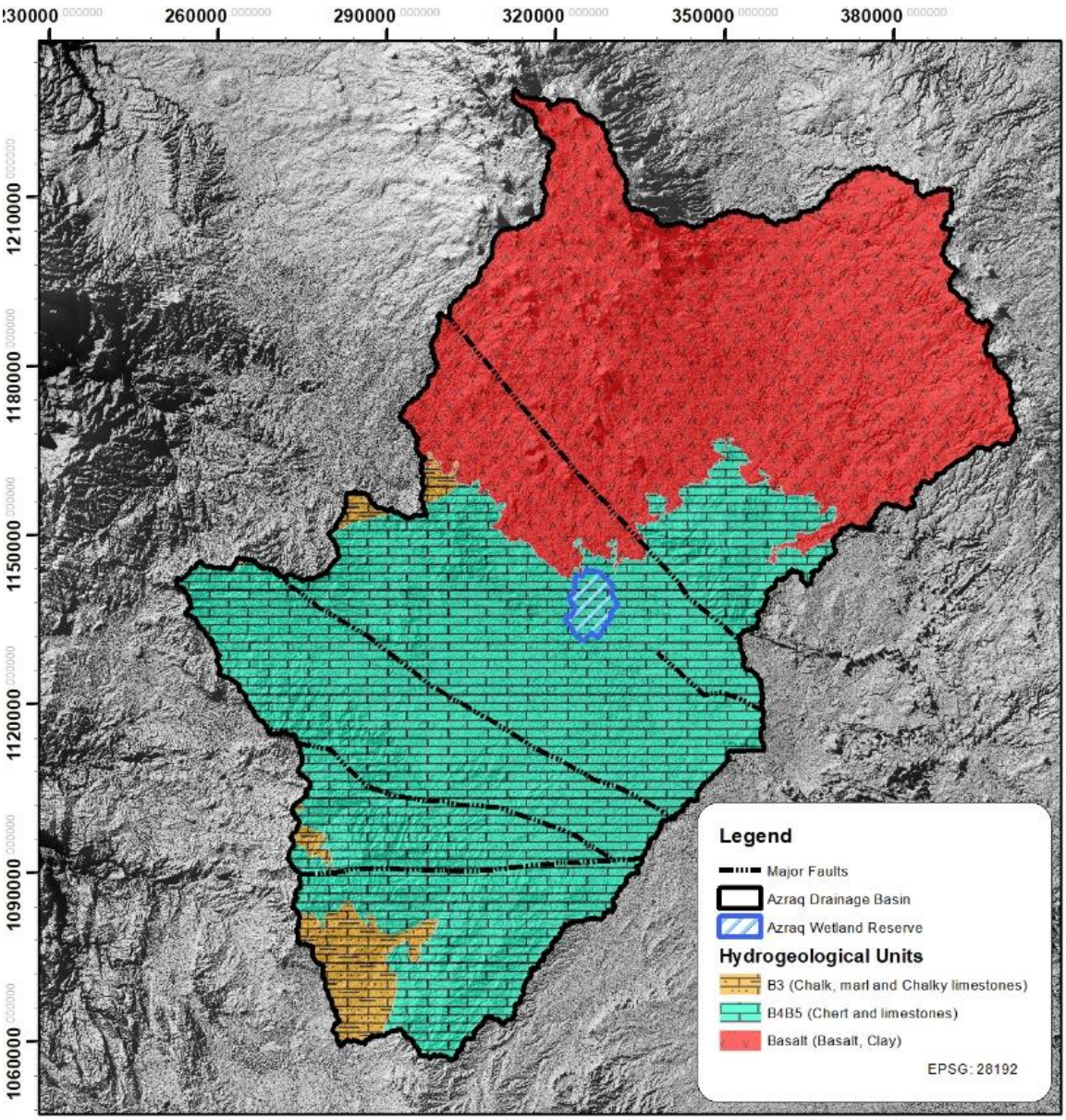

Figure 1-4. Hydrogeological units in the Azraq Basin.

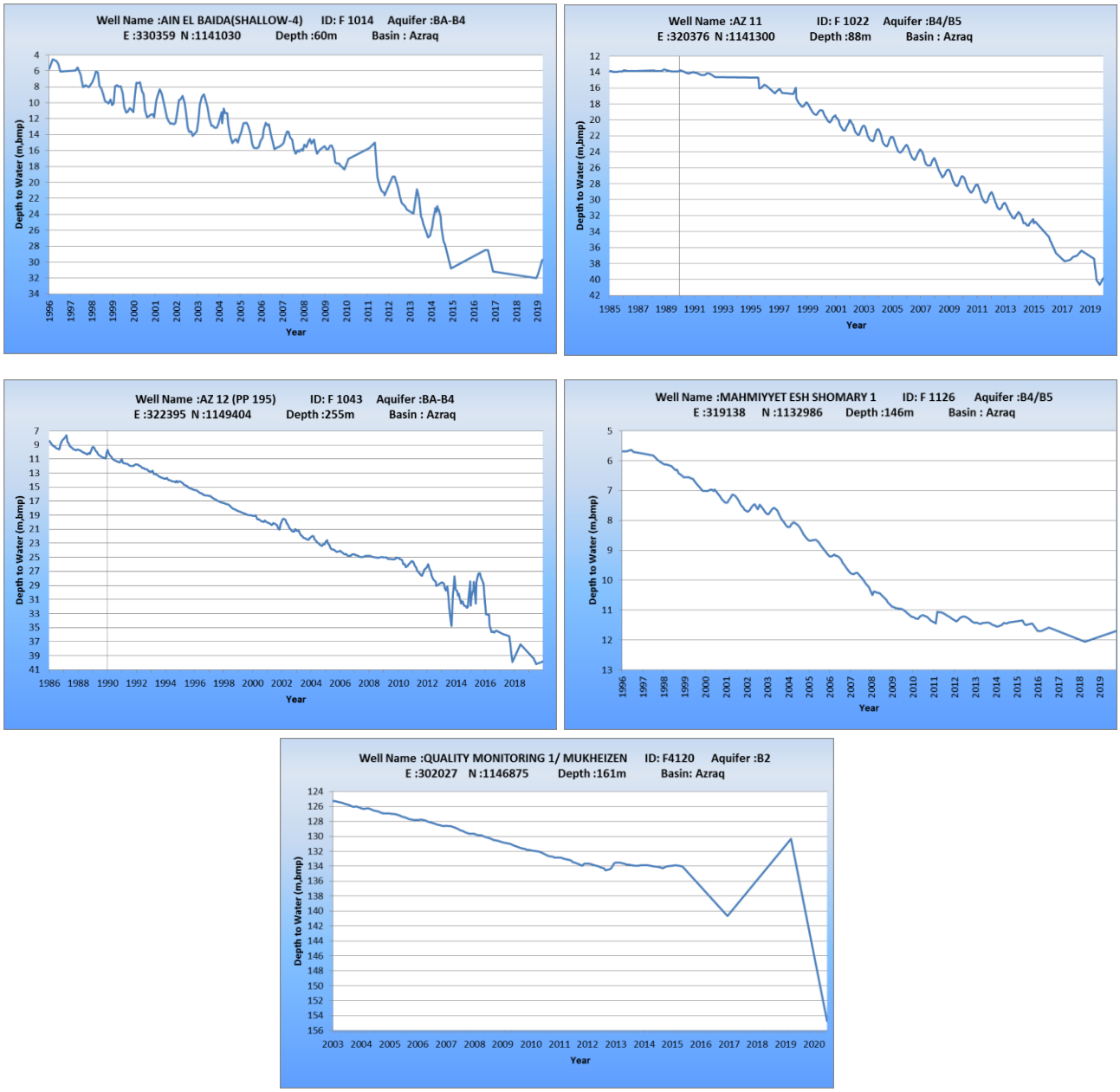

Figure 1-5. Groundwater piezometric levels observed in monitoring wells within the Azraq Basin for the last 15 years.

1.3.4 Land Use

The lands of the study area are owned by the forestry department of the Jordanian Ministry of Agriculture. Since 1977, the lands have been delegated to the Royal Society for the Conservation of Nature RSCN. Tribes living in the area are indigenous people of Druze, Chechens, and Bedouins. Azraq consists of eight districts: North Azraq, South Azraq, Tatweer Hadari, Ein Baida'a, Prince Hamza, Umm Al Masayel, Farms, and Mowafaq Al Salti air base. There was a recent demographic change in the region due to the political turmoil in the neighboring area led to the influx of Syrian refugees into Azraq and the establishment of a refugee camp with an estimated capacity of about 80 thousand refugees, which leads to the exit of some families and housing within the residential area to increase the population in the district and put great pressure on services and

infrastructure. Azraq became an attractive place to invest in agriculture due to cheap and easy land and water access, the availability of labor, and the presence of markets for export. However, uncertainty surrounding land ownership remains and affects agriculture investments. Some investors preferred to buy land legally, thus avoiding uncertainty and risking their investments. Others tried to buy land cheaply with hijjeh (muniments), aiming to legalize it later and expand agriculture. Facing this dual situation, it is difficult therefore to compare land prices as they are influenced by the existence of an official land deed or not, whether the land plot includes a well or not, whether the well is legal or not, its discharge, and water quality, and whether the land plot has access to electricity from the grid. Decreasing water table levels and the deterioration of water quality are also factors that can potentially reduce the value of the land and also increase uncertainty for agriculture in Azraq. Basalt outcrops are dominant in the northern part of the Azraq Basin, covering 37.7% of the total area which covers a large part of the ground surface between the towns of Azraq and Al-Ruwashid. In the southern portion, Chert Plains dominate covering 28.3% of the total basin surface area (Figure 1-6).

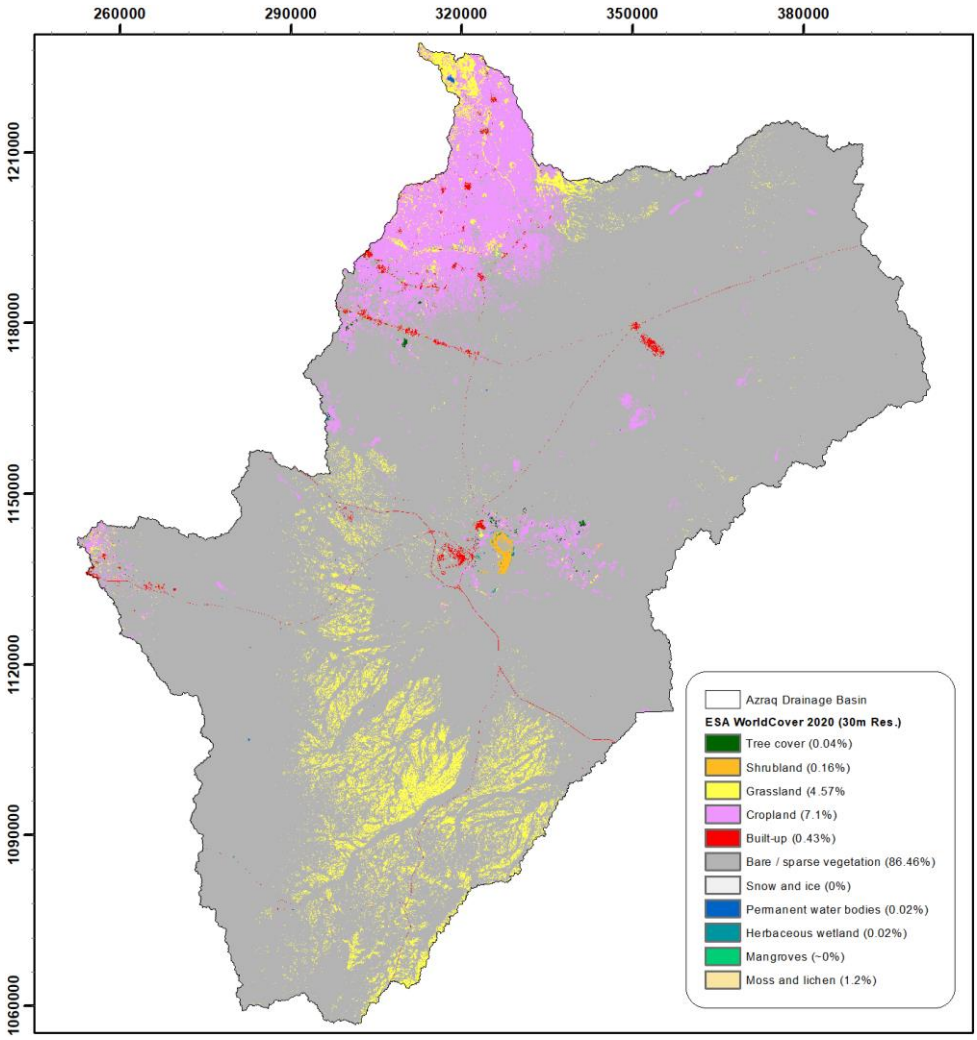

Figure 1-6. Land use/land cover in the Azraq Basin.

2. CONCEPTUAL MODEL

The following sections present the conceptualization of the Azraq Basin for the groundwater flow model based on previous studies, published information about the site, borehole logs, and geophysical survey results. Included are descriptions of the geologic aspects of the aquifer system, hydrologic boundaries, sources and sinks of groundwater, and information on hydraulic properties such as hydraulic conductivity and storage.

2.1 Aquifer System

Ibrahim and El-Naqa (2018) defined a possible stratigraphical sketch that represents the aquifer systems in the Azraq Basin (Figure 2-1). The upper aquifer system, composed of Quaternary sediments and basaltic rocks, is an unconfined aquifer. The aquifer consists essentially of four different members partly separated from each other by low permeability layers, partly directly connected. Two major groups of springs are located in the central part of the Azraq area comprising the main discharge outlets of the upper phreatic aquifer. The upper aquifer system is under water table conditions. The depth to the ground water table is from a few meters in the Azraq depression to 400 m in the northern parts of the catchment area. Groundwater elevations are the highest in the north-eastern part of the area, decreasing from 564 m a.s.l. to about 500 m a.s.l. towards the center of the basin. The general flow direction in the basalt aquifer is from NE to SW towards the center of the basin. The Jebel al-Arab Mountain in the north of the basin is the main recharge area for the Basalt aquifer.

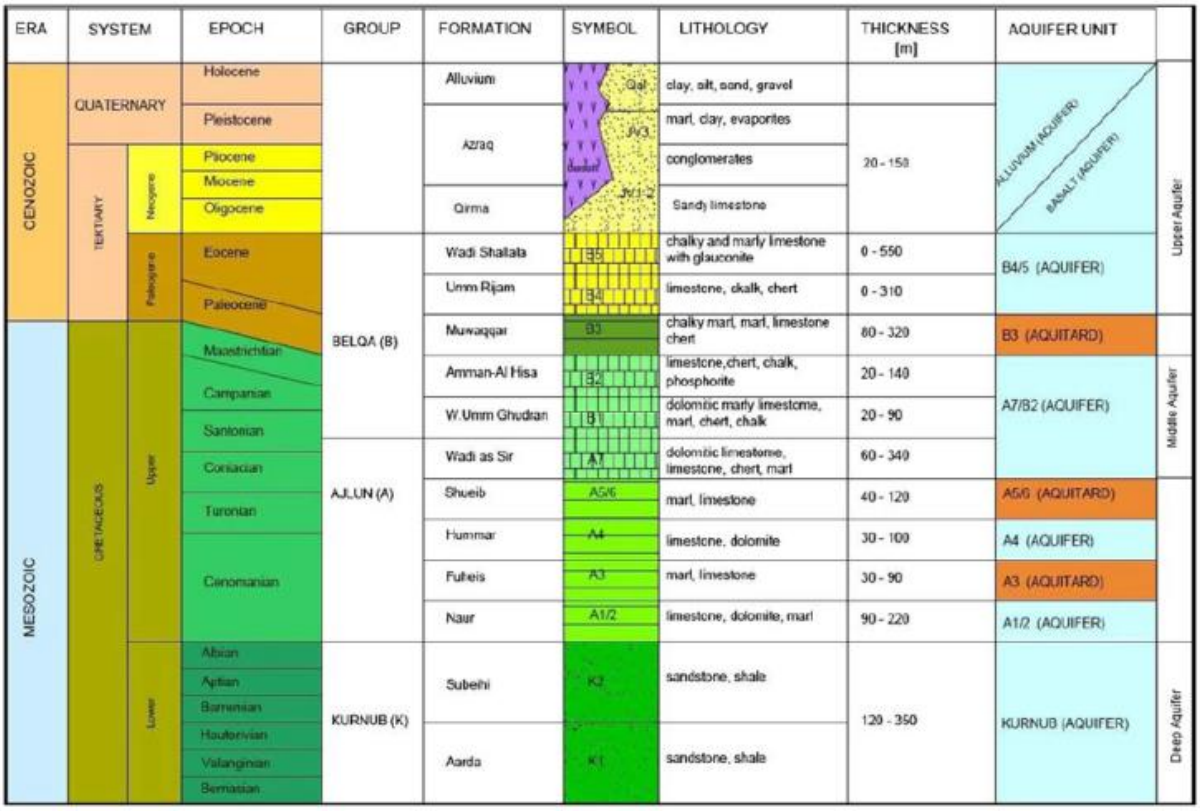

Figure 2-1. Stratigraphy and lithological classes of the aquifer systems in the Azraq Basin (Ibrahim and El-Naqa, 2018).

Underlying the basalt layer is the B4/B5 aquifer. The Paleogene B4 (Umm Rijjam) and B5 (Wadi Shallala) formations form a combined aquifer at the regional scale. The average thickness of the B4/B5 aquifer is approximately 230 m, and the maximum thickness, in the order of 970 m, including the overlying alluvium, is located in the Sirhan Graben (MWI and BGR, 2019) south of the Azraq Basin.

The middle aquifer system is locally known as Amman-Wadi as Sir (A7/B2) Aquifer System. The A7/B2 aquifer is the most important in Jordan and is extensively exploited (MWI & BGR, 2019). This aquifer is considered a confined aquifer due to the presence of a bituminous marl aquitard which limits its extension above (Figure 2-2). The middle aquifer system is exposed in the western part of Azraq and comprises chert, chalk, and silicified limestone. The potentiometric heads of this aquifer are 520 and 510 m a.s.l., respectively, at steady-state. They become 520 and 495 m a.s.l. in transient conditions, increasing the driving force of the upward flow.

The B3 aquitard separates the upper from the middle aquifer. Chalky to marly Paleogene limestones with minor intercalations of chert comprise this layer. Since most of the groundwater in Jordan is extracted from the underlying A7/B2 aquifer, the base of the B3 aquitard is generally well documented (MWI & BGR, 2019).

The aquifers are hydraulically interconnected, due to major faults as shown in Figure 2-2. Groundwater is flowing in different flow directions: water of the upper aquifer system flows from the north at Jebel El-Arab area toward the Qa-Azraq in the south, the water of the middle aquifer system flows from the west and the southwest (Zerqa and Mujib Basins) and from the east (Hammad Basin) to reach the Azraq depression, the water of the lower aquifer system flows from east to west to discharge in its lowest point at the Dead Sea Basin.

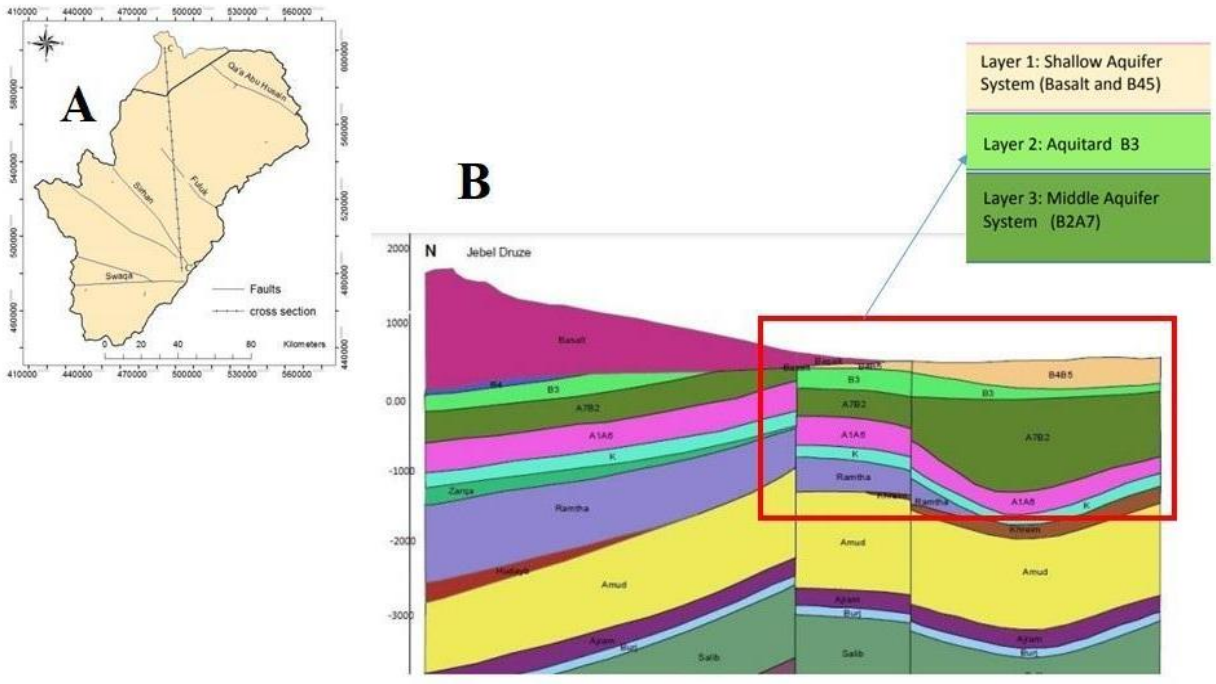

Figure 2-2. N-S geological cross-section of the Azraq Basin pilot site (modified from Alkhatib, 2017).

2.2 Hydrologic Boundaries

In a previous modeling study by Alkhatib et al. (2019), the boundary conditions of the flow model constructed for the Azraq Basin are shown in Figure 2-3. For the upper aquifer, the western model boundary was a no-flow boundary following the aquifer outcrop. The northern and north-western model boundary followed the groundwater divide in the basin and was also specified as a no-flow boundary. The north-eastern boundary was located along a streamline of the main groundwater flow direction and was set as a no-flow boundary like the water divide in the south-eastern border. The remaining boundaries of the upper aquifer system in the south and east were constant-head boundaries in the steady-state model, where the groundwater head was fixed at the values derived from the head distribution map prepared after Hobler et al. (2001). In the transient model by Alkhatib et al. (2019), general head boundaries were based on a head distribution map. For the middle aquifer system, the north-western, north-eastern, and south-eastern boundaries followed groundwater divides and were therefore specified as no-flow boundaries. The remaining model boundaries of the middle aquifer system are constant-head boundaries.

In the present study, hydrologic boundaries were conceptualized in a much simpler manner to avoid any uncertainties or misconceptions related to the actual state of the boundaries. The boundary conditions of the present flow model were set at the basin boundaries as no-flow boundaries assuming that groundwater divides are collocated with surface water basin boundaries.

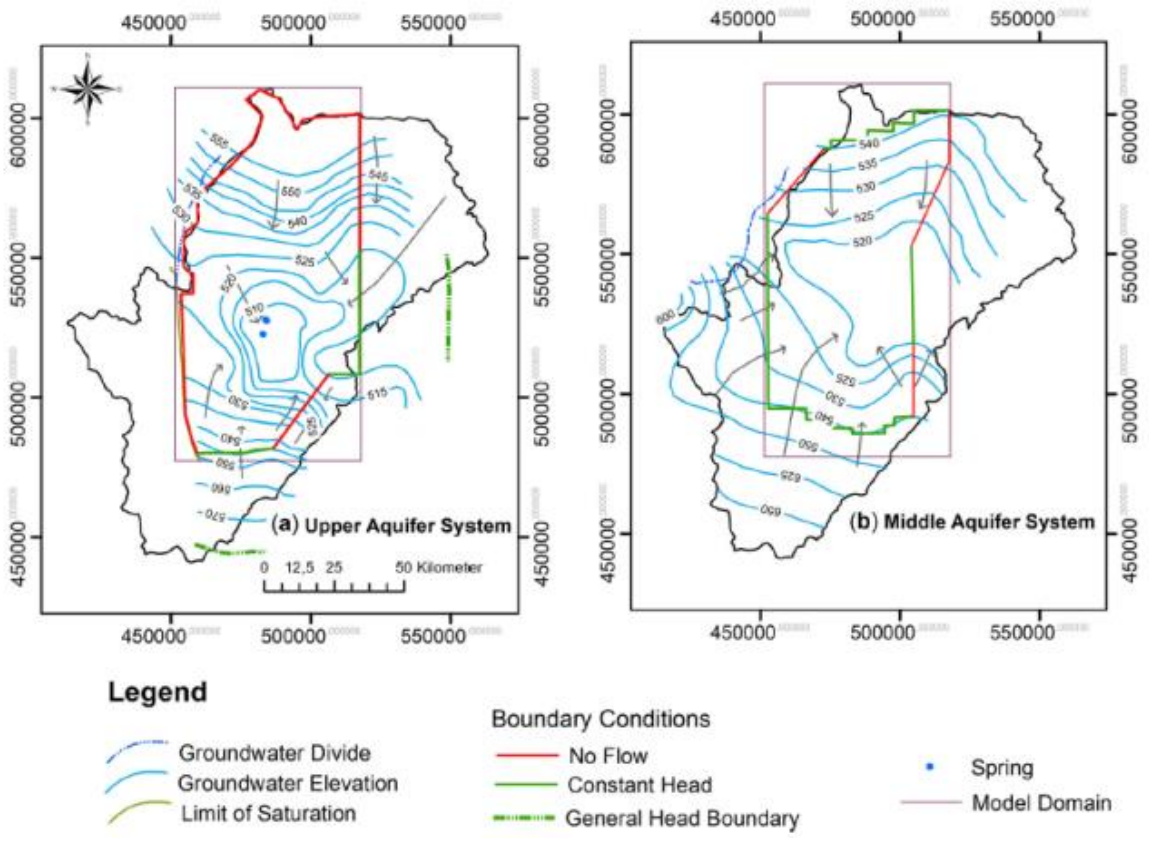

Figure 2-3. Model domain and boundary conditions for the upper and middle aquifer systems from the previous modeling study by Alkhatib et al. (2019).

2.3 Hydraulic Properties

Table 2-1 summarizes hydraulic conductivity and specific yield estimates obtained from model calibration of the flow model by Alkhatib et al. (2019). Here the formation labeled as "Middle Aquifer" refers to model layer 4, which represents aquifer A7/B2. Hydraulic conductivity estimates for the hydrogeological units in the Azraq Basin were published in various studies. The findings of one of these studies are summarized in Table 2-2.

Table 2-1. Calculated hydraulic conductivity and specific yield of different aquifers in the Azraq Basin (Alkhatib et al., 2019).

Formation	*K* [m/s]	Sy [−]
Upper aquifer, basalt	1.7E-4	0.002
Upper aquifer, carbonate B45	1.4E-5, 3.4E-4	0.02
Middle aquifer	2.8E-6, 3.4E-4	–

Table 2-2. Geological and hydrogeological classification of the aquifers in the Azraq Basin (Rimawi, 1985).

Epoch	Age	Group	Formation	Symbol	Rock type	Thickness (m)	Aquifer potentiality	Permeability (m/s)
Tertiary	Holocene	Balqa	Wadi Fill	All	Soil, sand and gravel	10-40	Good	2.4 x10 $^{-7}$
	Pleistocene		Basalt	V	Basalt. clay	0-50	Good	-
			Wadi Shallala	B_5	Chalk, marly limestone with gluconite	0-555	Good	
			Umm Rijam	B_4	Chert and limestones	0-311	Good	
Upper Cretaceous	Maestrichtain		Muwaqqar	B_3	Chalk, marl and chalky limestone	60-70	Poor	-
	Campanian		Amman	B_2	Chert, limestone with phosphate	80-120	Excellent	10 $^{-5}$- 3 x 10^{-4}
	Santonian		Ghudran	B_1	Chalk, marl and marly limestone	15-20	Poor	-
	Turonian	Ajlun	Wadi Sir	A_7	Hard crystalline limestone dolomitic and some chert	90-110	Excellent	1x10^{-7} - 1x10^{-4}
	Cenomanian		Shueib	A_{5-6}	Light grey limestone interbeded with marls and marly limestone	75-100	Fair to poor	6.3 x10^{-5} -7.2 x10^{-4}
			Hummar	A_4	Hard dense limestone and dolomitic limestone	40-60	Good	8.1 x 10^{-7} - 7.6 x10^{-4}
			Fuheis	A_3	Gary and olive green soft marl, marly limestone and limestone	60-80	Poor	5.3 x 10^{-7} - 1.7 x 10^{-5}
			Na'ur	A_{1-2}	Limestone interbeded with a thick sequence of marl and marly limestone	150-220	Poor	2 x 10^{-8} - 3.1 x 10^{-5}
Lower Cretaceous	Albian – Aptian		Kurnub	K	Massive white and varicolored sandstone with layers of reddish silt and shale	300	Good	6.9 x 10^{-3}- 5.2 x 10^{-2}

2.4 Sources and Sinks

2.4.1 Recharge

Groundwater recharge represented the main input component to the groundwater system. Groundwater recharge was related to rainfall in the basin. Leakage of water from each wadi (dry riverbed and its drainage area, which contains water only during heavy rain) could not be included in the model because data or estimations were not available.

Precipitation in the study area occurs typically in the form of rainfall storms that have high intensity. As the precipitation varies considerably within the Azraq basin (mean rainfall > 500 mm/yr in the north and < 50 mm/yr in the south), the spatial distribution of groundwater recharge is in parallel expected to be heterogeneous. Therefore, recharge with an average long-term rate of 1.7 mm/yr occurs mainly in the north of the basin and drops below 1 mm/yr in the south and east of the basin (Al-Kharabsheh, 1995). Furthermore, mountain-front recharge from the north is also a known factor that supplements the aquifers in the basin. Another study conducted for the Azraq Basin found that in areas with rainfall of more than 75 mm/yr recharge is approximately 3.3% of the total rainfall (Margane et al., 2002).

2.4.2 Extraction Wells

Most groundwater extraction occurs around the Azraq oasis area for agricultural purposes through public water supply wells owned by the government (AWSA wellfield). Beginning in 1981, 1.5 Mm^3/yr of groundwater was pumped from the wellfield in the center of the basin for domestic purposes. Pumping rates increased gradually to 40 Mm^3/yr by the year 2013, firstly to meet the increasing water demand of the capital Amman and secondly, to provide irrigation water for agriculture.

The annual rate of pumped water to the wetland between the periods of 1996-2021 decreased significantly (Figure 2-4) because AWR management was not in control of the pumping operation. The MWI is in charge of the pumping station close to the AWR. However, the authority has given in the past priority to domestic water supply purposes during water shortage time in the summer. The increasing number of inhabitants (refugee camps), the number of wells, ponds, and dams on the surface water runoff pathways, in companion with the high temperatures in summer, all directly or indirectly reduced the amount of water received by the AWR.

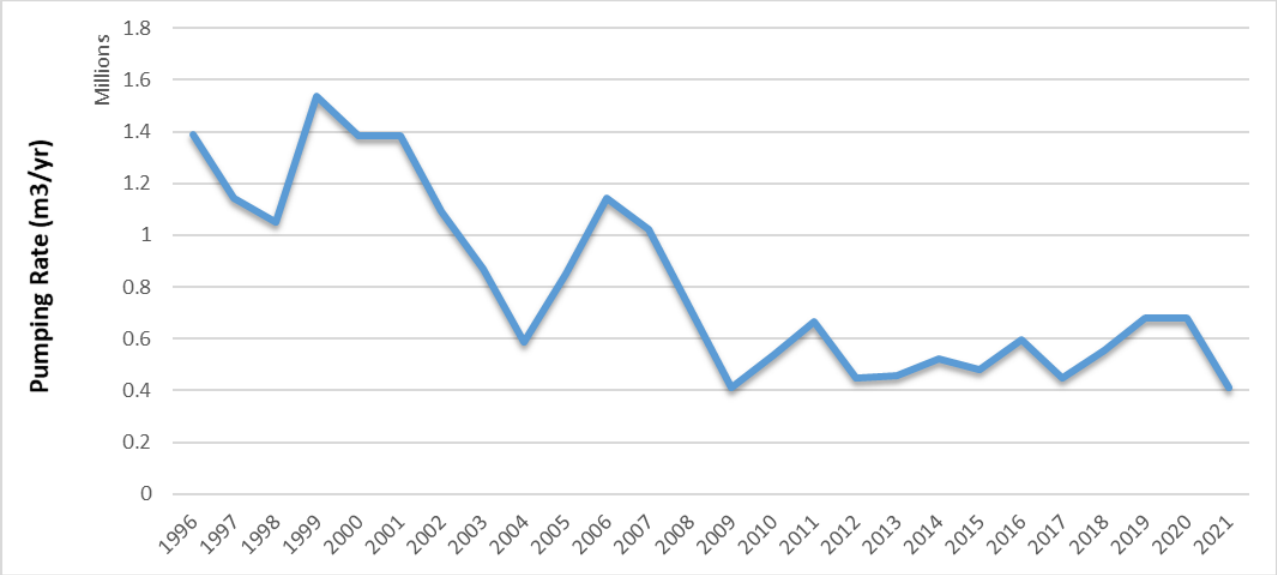

Figure 2-4. Rates of groundwater pumped from the MWI well to the wetland during the period 1996 – 2021.

The MWI pumping station is considered as the only one within the boundaries of the wetland since 1994, which was established within an agreement signed between the Ministry of Water and the Royal Society for the Conservation of Nature. This agreement requires the Ministry of Water to pump 1.5-2.5 Mm^3/yr to the wetland to meet the needs of the water bodies and sustain the vital system in it. However, the annual pumping rate has not yet reached the agreed value, due to the lack of separate infrastructure for the main station in Azraq and the increasing demand for water for domestic and other uses in the area. So far, the annual pumping rate has not exceeded 0.55 - 0.65 Mm^3/yr.

3. MODEL CONSTRUCTION

Groundwater flow in the Azraq Basin is simulated using the three-dimensional finite-difference groundwater flow model MODFLOW-2005. The model was constructed with Modelmuse 5.1.1 (Winston, 2022), an interface of MODFLOW-2005, and various other models developed and maintained by the U.S. Geological Survey, USGS. The governing equation that represents the three-dimensional movement of constant-density groundwater in saturated porous media is:

$$\frac{\partial}{\partial x}\left(K_{xx}\frac{\partial h}{\partial x}\right)+\frac{\partial}{\partial y}\left(K_{yy}\frac{\partial h}{\partial y}\right)+\frac{\partial}{\partial z}\left(K_{zz}\frac{\partial h}{\partial z}\right)+W=S_s\frac{\partial h}{\partial t} \qquad \text{(Equation 1)}$$

where

K_{xx}, K_{yy}, and K_{zz} are hydraulic conductivities along the x, y, and z coordinate axes, which are assumed to be parallel to the major axes of hydraulic conductivity (L/T);

h is the hydraulic head (L);

W is a volumetric flux per unit volume representing sources and/or sinks of water, with W <0.0 for flow out of the aquifer system, and W > 0.0 for flow into the system (T^{-1});

S_s is the specific storage of the porous medium (L^{-1}); and

t is time (T).

Equation 1 describes groundwater flow under transient conditions in a heterogeneous and anisotropic porous medium. This equation, together with specifications of flow and/or head conditions at the boundaries (boundary conditions), constitutes a mathematical representation of a groundwater flow system. As the analytical solutions of Equation 1 are rarely possible, except for very simple systems, the equation system must be solved by numerical methods. The numerical approach of MODFLOW is the finite-difference method, where Equation 1 is replaced with an algebraic equation, thereby approximating the partial differential equation.

3.1 Spatial and Temporal Discretization

The three-dimensional model grid is based on a variable spatial resolution ranging from 500 to 2500 m and consists of 4 layers, 98 columns, and 114 rows. The model grid is refined in the center of the Azraq Basin, where the wetland catchment is located (Figure 3-1). The smoothing factor for grid refinement is selected as 1.2. The model grid contains a total of 24943 active cells in all 4 model layers, the number of active cells being different in each layer due to the inactivation of some cells coinciding with outcropped formations. The model domain covers a surface area of 12,053 km^2. The projection used for geospatial data management in Modelmuse was Palestine 1923 datum, Palestine Belt Universe Transverse Mercator projection. The grid rotation angle is 0 degrees. Numerical model spatial units were in meters.

The flow model was vertically discretized into four model layers, which have extents that were based on the delineation of hydrogeological units in the conceptual model. Contour maps of these layers were obtained from the MRI as part of a nationwide dataset that was first produced in 1995. This dataset was later updated with information from new boreholes (MWI and BGR, 2019). These contour maps show the estimated bases of major hydrogeological units in the Azraq Basin. The top surface of the model was representative of the

mean land surface elevation in each model grid cell. The mean land surface elevation was determined based on a 38.2-m resolution DEM for the model area and was assigned as the top elevation of the uppermost model layer. The uppermost layer (L1) represented the outcropping basalt aquifer, which forms an unconfined aquifer. The next layer (L2) was representative of the B4/B5 aquifer, which is composed of marly limestone and chalk. The aquitard unit B3 is assigned as Layer 3 (L3) consisting of chalky marl, marl, and less permeable limestone. The following layer (L4) is a confined limestone aquifer, representing the A7/B2 unit. The bottom of the model was represented by the top of the Shueib formation (A5/A6 aquitard). Model layer bottom elevations for each layer are shown in Figure 3-2.

Different views of the 3-D flow model grid are shown in Figure 3-3. The Fuluk Fault causes layer surfaces with abrupt changes near the fault zone. This discontinuity is visible in cross-sections of the model grid. As the hydraulic behavior of the Fuluk Fault is not certain the fault zone was not considered in the model explicitly. However, the fault still appears in the model grid as abruptly changing layers although considerably smoothed.

All model layers except L1 were set as confined-type layers (LAYTYP = 0). The layer type for L1 was set as “convertible” with the wetting option activated. The Layer-Property flow package (LPF) of MODFLOW (Harbaugh, 2005) was chosen to specify properties controlling flow between grid cells in the model.

The flow model was temporally discretized into transient stresses using blocks of time called “stress periods”, within which all hydrologic stresses are constant and model output applies to the end of each stress period. The model was discretized into 96 months of stress periods spanning over the simulation period that begins in January 2013 and ends in December 2020. The simulation period was defined, firstly to cover the time frame of the InSAR-derived land subsidence analysis period. Secondly, the time interval of the available data related to hydrological stresses such as recharge and pumping was relevant. Stress periods of the model represented monthly conditions. Hydrological stresses on the aquifers during the transient stress periods were representative of the net groundwater recharge rate, groundwater withdrawal rates through pumping wells, and evapotranspiration. The constant time steps of the model were assigned using units of days, consequently resulting in 2922 days of simulation time.

Figure 3-1. Numerical flow model grid for the Azraq Basin with variable spatial resolution. Panels show active cells for each model layer.

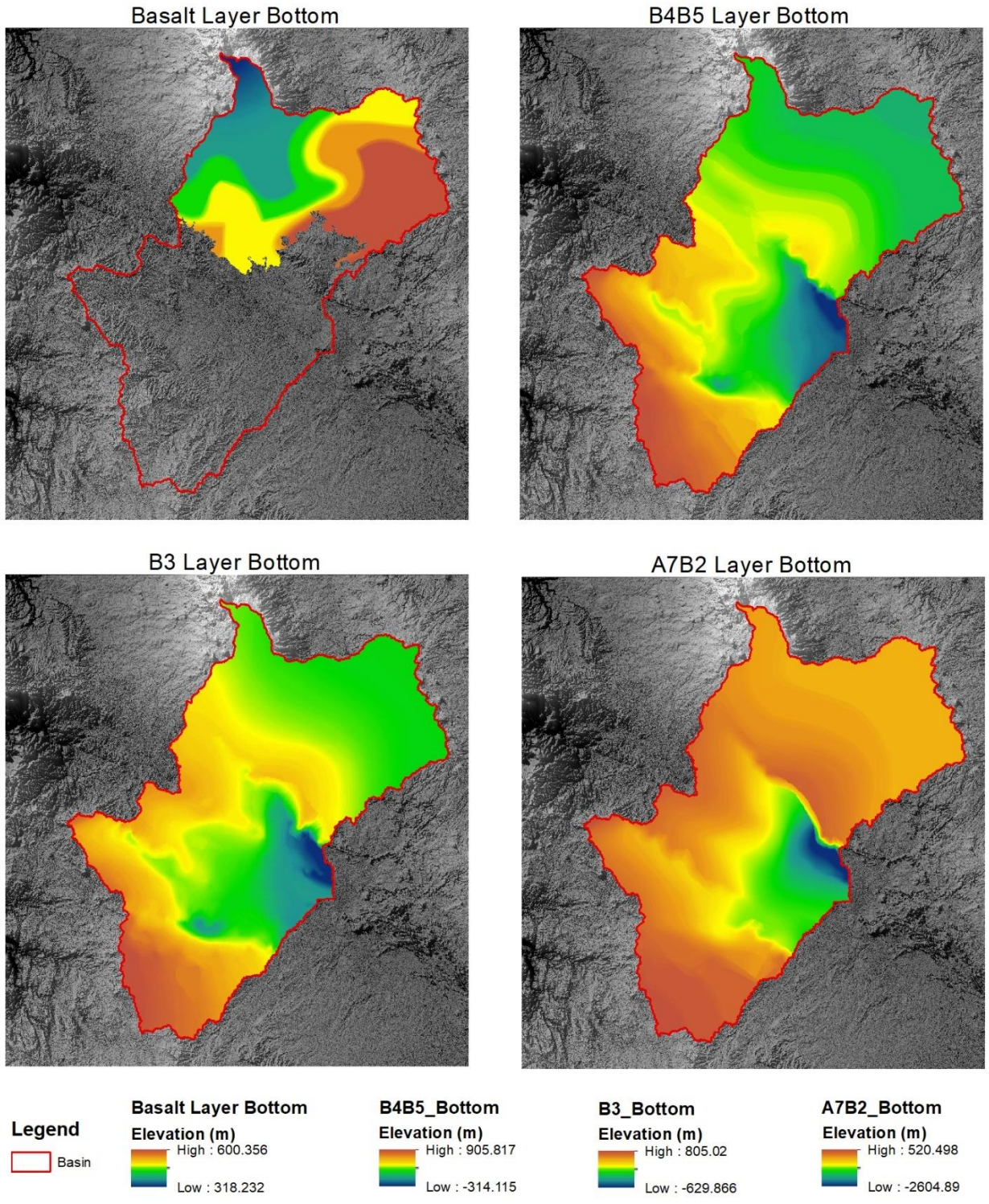

Figure 3-2. Base elevations of each model layer of the Azraq Basin flow model.

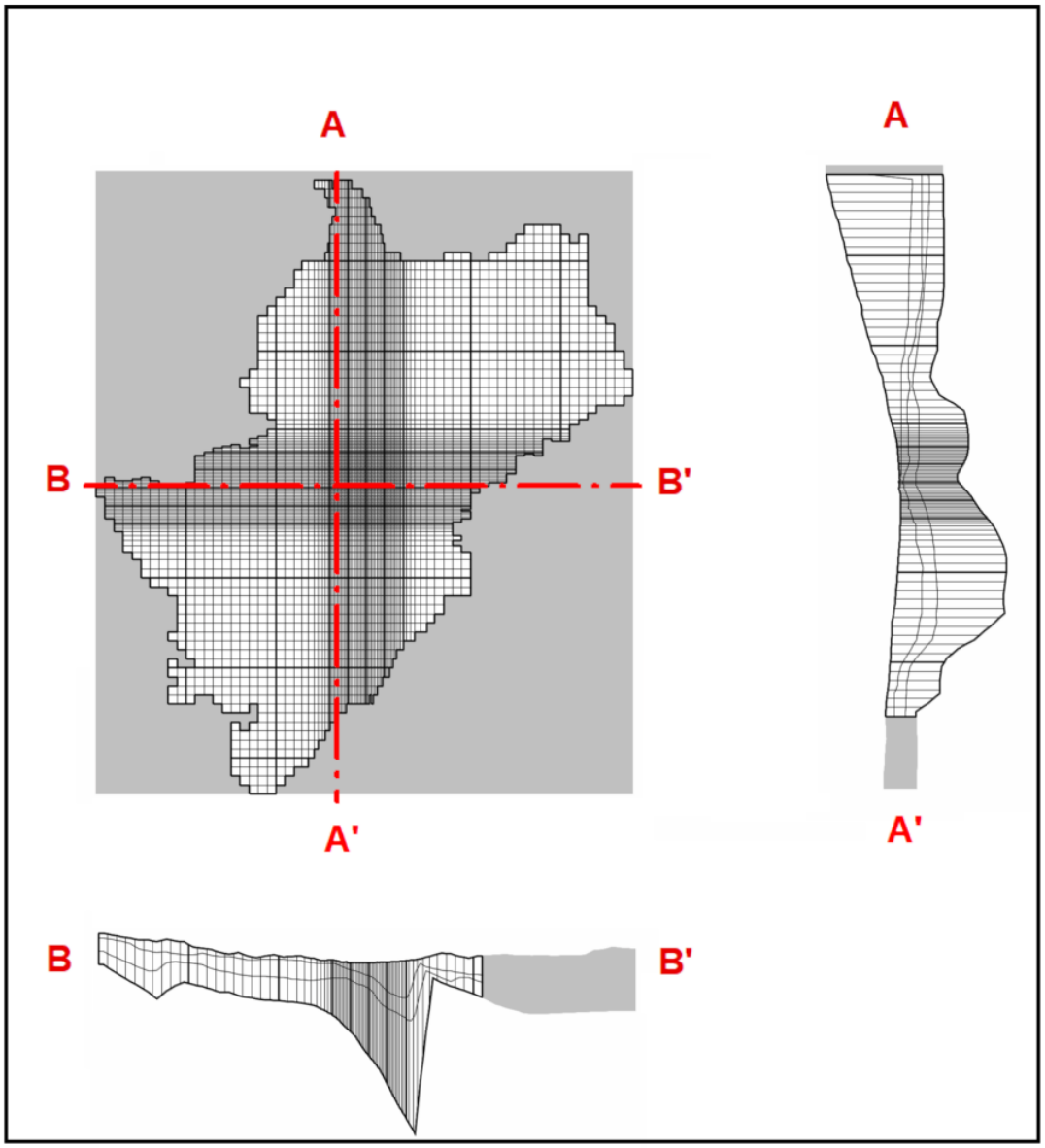

Figure 3-3. Plan view and cross-sections of the flow model grid for the Azraq Basin.

3.2 Initial Conditions

The initial head distribution of the flow model was determined by interpolating groundwater level observations from January 2013 over the model domain. Several different interpolation methods were tried until a satisfactory map of the initial potentiometric surface was obtained. The map of the initial head distributions assigned to each model layer is shown in Figure 3-4.

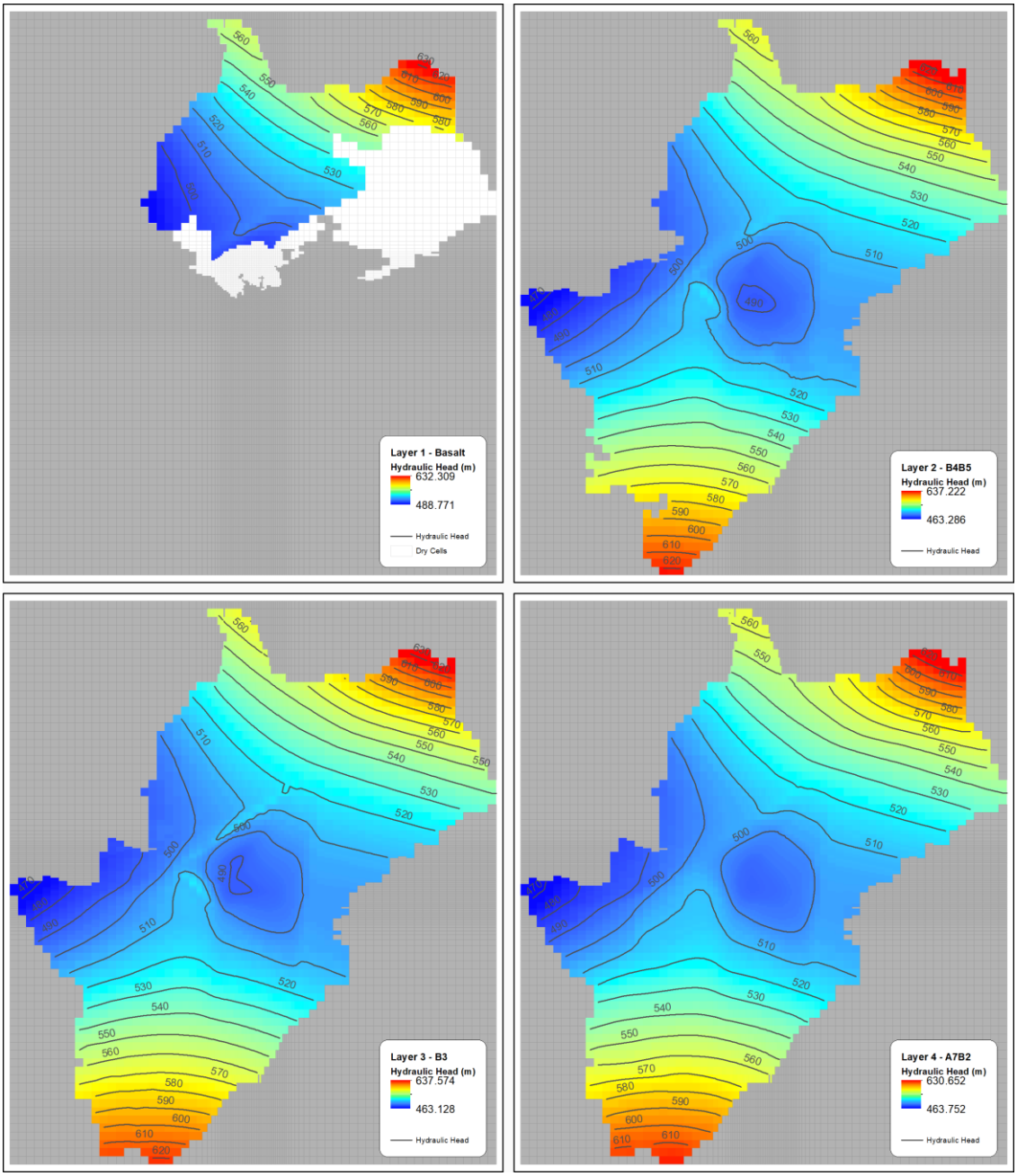

Figure 3-4. Initial conditions representing the head distributions in January 2013 were assigned to model layers 1 through 4.

3.3 Boundary Conditions

All model boundaries in all layers were set as no-flow boundaries with the assumption that the surface water basin boundaries are collocated with the groundwater basin boundaries. For this assumption to be valid the model boundaries must be sufficiently far from the AOI, which is the Azraq Wetland Reserve Area. Since no-flow boundary conditions can constrain the resulting head distributions, the effect of the boundaries on the solution was tested. As a result of this test, using a general-head boundary instead of a no-flow boundary

caused no significant change in the solution for the AOI and its near vicinity. The mean absolute error between these two solutions was 0.32 m in the AOI.

3.4 Hydraulic Parameters

Hydraulic conductivity and the storage coefficient are the hydraulic parameters of the flow model. Transmissivity data points were estimated using the empirical relationship from El-Naqa (1994):

$$T = 60878.2\left(\frac{Q}{s}\right)^{0.917} \qquad \text{(Equation 2)}$$

where T is the transmissivity estimation (m^2/d); (Q/s) the specific capacity of the well ($m^3/s/m$). Specific capacity data was available for 164 wells that are located inside the Azraq Basin (Table 3-1). Drawdown was recorded during the initial development of the wells, where the lithology and the elevation of the screened interval were known. Data points were assigned to a single model layer even if the well screen spans over multiple aquifers. Consequently, 100 data points were assigned to Layer 2 (B4/B5), and 64 data points were assigned to Layer 4 (A7/B2). The transmissivity estimations for model layers 2 and 4 and their distributions within the model domain are depicted in Figure 3-5. Transmissivity estimations were then divided by their corresponding well screen lengths to obtain hydraulic conductivities. Interpolation of point estimates of hydraulic conductivities to the entire model layer resulted in heterogeneous K distributions for Layers 2 and 4. The initial horizontal hydraulic conductivity of Layer 1 was assumed to be homogeneous with a value of $K_x = K_y =$ 14.688 m/d. Also, the initial horizontal hydraulic conductivity of the aquitard (Layer 3) was assumed to be homogeneous with a value of $K_x = K_y =$ 0.003 m/d. The initial vertical anisotropy ratio was assumed as K_x/K_z = 10. The simulated flow of groundwater between model cells in adjacent model layers is controlled by the vertical conductance term which is calculated within MODFLOW from the thickness of each model layer between its node and common layer contact and the vertical hydraulic conductivity of each layer. Initial assignments of hydraulic conductivities used in the model are summarized in Table 3-2.

Initial storage coefficients were chosen after an in-depth review of previous modeling studies and other study reports. Parameter values that were assigned in the model are provided in Table 3-2. Storage coefficients were initially assigned to all layers as homogenous parameters. The parameter value for Layer 1 represents the specific yield instead of the specific storage.

Table 3-1. Database of hydraulic conductivities (m/d) estimated using specific capacities of wells in the Azraq Basin.

Well ID	Easting	Northing	Aquifer	Hydraulic Cond.
	Epsg:28192		-	m/d
CD1250	274701	1108573	B2/A7	0.300
CD3078	275456	1109168	B2/A7	1.172
CD3092	274581	1107623	B2/A7	1.557
CD3094	274956	1110043	B2/A7	0.152
F 1002	316503	1130075	B4/B5	16.553
F 1003	317640	1126170	B4/B5	0.179
F 1004	321083	1129042	B4/B5	2.527
F 1006	318796	1126932	B4/B5	0.140
F 1010	340916	1137369	B4/B5	9.885
F 1011	341704	1133422	B4/B5	0.905
F 1012	342224	1133782	B4/B5	1.245
F 1013	340034	1137112	B4/B5	5.761
F 1014	330442	1141071	B4/B5	5.458
F 1022	320459	1141341	B4/B5	244.048
F 1023	320763	1139640	B4/B5	66.794
F 1024	321873	1138522	B4/B5	28.131
F 1026	322113	1137982	B4/B5	35.345
F 1028	321571	1150559	B4/B5	20.514
F 1029	322208	1150363	B4/B5	21.060
F 1030	322233	1149880	B4/B5	21.673
F 1031	321561	1151075	B4/B5	6.698
F 1032	321317	1151242	B4/B5	2.239
F 1033	321914	1151493	B4/B5	20.405
F 1034	323329	1149398	B4/B5	68.650
F 1035	321587	1152486	B4/B5	6.582
F 1036	323302	1150237	B4/B5	2.377
F 1037	322824	1149906	B4/B5	17.319
F 1038	322498	1149203	Basalt	699.557
F 1039	321800	1147839	B4/B5	18.320
F 1040	321293	1148395	B4/B5	77.674
F 1041	320854	1147979	B4/B5	11.401
F 1042	321252	1146966	B4/B5	3.788
F 1043	322478	1149445	B4/B5	4.502
F 1044	322804	1147148	B2/A7	0.263
F 1045	305263	1153838	B4/B5	0.414
F 1047	356494	1175410	B4/B5	0.151
F 1054	296482	1136742	B3	0.076
F 1059	321134	1141961	B4/B5	12.239
F 1061	329804	1127357	B4/B5	0.024
F 1062	320565	1120912	B4/B5	1.352
F 1063	341413	1107662	B4/B5	0.067
F 1066	293953	1125067	B4/B5	1.533

Well ID	Easting	Northing	Aquifer	Hydraulic Cond.
	Epsg:28192		-	m/d
F 1077	321003	1166070	B4/B5	2.295
F 1125	324003	1173910	B4/B5	7.767
F 1126	319221	1133028	B4/B5	0.052
F 1127	335684	1144041	B4/B5	2.395
F 1130	344834	1117362	B4/B5	0.109
F 1144	305657	1146721	B4/B5	90.208
F 1145	305672	1146716	B2/A7	1.616
F 1155	313391	1147580	B4/B5	3.163
F 1162	318383	1141741	B4/B5	1.544
F 1169	315824	1142832	B4/B5	1.977
F 1170	316736	1144318	B4/B5	8.404
F 1172	302182	1133002	B4/B5	0.934
F 1174	314974	1131481	B4/B5	2.048
F 1175	314125	1131567	B4/B5	0.666
F 1176	312042	1130515	B2/A7	0.080
F 1177	309993	1128992	B4/B5	0.872
F 1178	312033	1128601	B4/B5	1.161
F 1179	313098	1135212	B4/B5	0.313
F 1185	309133	1137017	B4/B5	0.509
F 1194	293872	1125092	B2/A7	39.127
F 1207	332583	1143541	B4/B5	4.784
F 1212	336704	1169960	Basalt	0.281
F 1221	341834	1117362	B4/B5	0.105
F 1223	341067	1118102	B4/B5	0.338
F 1225	305897	1133237	B2/A7	1.301
F 1226	314025	1148154	B4/B5	1.246
F 1227	332083	1132042	B4/B5	0.920
F 1229	334383	1131442	B4/B5	1.171
F 1230	341510	1129186	B4/B5	0.483
F 1231	318973	1114043	B4/B5	0.334
F 1240	323754	1129217	B2/A7	0.104
F 1242	312913	1093772	B4/B5	2.049
F 1243	295722	1145991	B2/A7	0.021
F 1246	326013	1144191	B4/B5	16.225
F 1249	331263	1144401	B4/B5	17.585
F 1257	336304	1141241	B4/B5	7.220
F 1262	343494	1134842	B4/B5	4.052
F 1268	305442	1146741	B4/B5	1.997
F 1269	309133	1148466	B4/B5	0.021
F 1270	306312	1146741	B4/B5	0.197
F 1271	320743	1139342	B4/B5	13.374
F 1274	300232	1134872	B2/A7	0.124
F 1282	358084	1177700	B4/B5	1.879

Well ID	Easting	Northing	Aquifer	Hydraulic Cond.
	Epsg:28192		-	m/d
F 1286	312564	1092656	B4/B5	20.892
F 1286	312564	1092656	B4/B5	25.424
F 1287	342832	1106367	B4/B5	0.279
F 1288	342634	1106023	B4/B5	0.590
F 1290	342275	1104042	B4/B5	0.285
F 1293	321253	1142641	B4/B5	12.772
F 1295	319833	1140641	B4/B5	1.117
F 1296	319743	1138712	B4/B5	4.962
F 1298	355976	1176310	B4/B5	0.402
F 1303	330528	1154395	B4/B5	2.695
F 1306	322823	1147151	B2/A7	0.583
F 1307	306082	1067045	B4/B5	0.325
F 1308	321003	1165910	B4/B5	0.523
F 1314	329833	1097043	B4/B5	0.024
F 1316	358084	1177685	B4/B5	0.822
F 1318	371085	1188740	B2/A7	0.881
F 1334	350384	1180040	B4/B5	0.683
F 1336	288082	1127042	B2/A7	0.113
F 1346	293632	1120002	B2/A7	0.514
F 1348	270246	1131995	B2/A7	0.226
F 1350	331883	1140441	B2/A7	1.798
F 1352	310283	1149141	B2/A7	9.576
F 1354	332733	1156041	B2/A7	1.377
F 1356	329458	1173065	B2/A7	0.122
F 1360	295982	1146341	B2/A7	15.496
F 1362	299677	1082524	B2/A7	2.271
F 1364	279711	1085634	B2/A7	2.648
F 1366	284972	1100808	B2/A7	13.126
F 1368	358184	1199964	B2/A7	7.443
F 1370	259581	1135292	B2/A7	0.188
F 1383	276681	1111363	B2/A7	0.290
F 1387	254930	1142011	B2/A7	0.507
F 1393	274881	1097723	B2/A7	0.471
F 3209	262081	1139541	B2/A7	0.047
F 3222	320421	1152184	B4/B5	229.701
F 3530	321083	1174740	B4/B5	5.589
F 3579	259681	1134892	B2/A7	0.163
F 3589	260281	1135792	B2/A7	0.363
F 3590	261021	1136522	B2/A7	0.639
F 3592	259206	1139116	B2/A7	0.395
F 3592	259206	1139116	B2/A7	0.577
F 3592	259206	1139116	B2/A7	0.046
F 3592	259206	1139116	B2/A7	0.068

Well ID	Easting	Northing	Aquifer	Hydraulic Cond.
	Epsg:28192		-	m/d
F 3594	257981	1139641	B2/A7	0.133
F 3755	261181	1134442	B2/A7	0.132
F 3756	263386	1133827	B2/A7	0.992
F 3757	264616	1133332	B2/A7	0.863
F 3758	265976	1132957	B2/A7	0.331
F 3759	267814	1132605	B2/A7	3.453
F 3760	267907	1133830	B2/A7	0.162
F 3875	318720	1139902	B4/B5	1.493
F 3900	300222	1144012	B2/A7	2.638
F 3903	352084	1180040	B4/B5	0.600
F 3910	263461	1135712	B2/A7	0.162
F 3922	259781	1137142	B2/A7	0.178
F 3923	261881	1137542	B2/A7	0.025
F 3925	261881	1135942	B2/A7	0.135
F 3927	256341	1142531	B2/A7	0.110
F 3935	327883	1172640	B4/B5	73.546
F 3947	320865	1148011	B4/B5	0.515
F 3979	310233	1149141	B4/B5	0.775
F 3988	257081	1138042	B2/A7	0.035
F 4034	262131	1137517	B2/A7	0.042
F 4035	258241	1139091	B2/A7	0.092
F 4080	299482	1082464	B2/A7	1.384
F 4087	263021	1136542	B2/A7	0.870
F 4088	321619	1139749	B4/B5	265.786
F 4098	320808	1147967	B4/B5	0.953
F 4136	261681	1134842	B2/A7	0.065
F 4141	321566	1150554	B4/B5	10.431
F 4164	269387	1132225	B2/A7	0.353
F 4166	321108	1149405	B4/B5	355.403
F 4202	335697	1175156	B2/A7	0.035
F 4228	270581	1133042	B2/A7	0.380
F 4232	336326	1145129	B4/B5	1.521
F 4246	302082	1117542	B4/B5	0.048
F 4269	265361	1133532	B2/A7	0.174
F 4281	260281	1135792	B4/B5	0.191
F 4303	322143	1139110	B4/B5	4.200
F 4321	265644	1131934	B2/A7	0.261
F 4333	322441	1149392	B4/B5	28.335
F 4352	299266	1147110	B2/A7	1.159
F 4388	340488	1176788	B2/A7	0.065
F 4392	321401	1169150	B2/A7	5.696
F4389	346609	1133723	B2/A7	0.092
F4391	345127	1138992	B2/A7	0.458

Table 3-2. Summary of initial hydraulic parameter values by model layer.

	Horizontal Hydraulic Conductivity (m/d)			Vertical Hydraulic Conductivity (m/d)			Storage Coefficient (m^{-1}) / Specific Yield (-)
	Min	Median	Max	Min	Median	Max	
Layer 1 Basalt aquifer	14.688			1.469			0.002
Layer 2 B4/B5 aquifer	0.046	2.830	280.6	$4.6 \cdot 10^{-3}$	0.283	28.06	$1.73 \cdot 10^{-5}$ – 0.02
Layer 3 B3 aquitard	0.003			$3 \cdot 10^{-4}$			10^{-5}
Layer 4 A7/B2 aquifer	0.046	1.280	34.964	$4.6 \cdot 10^{-3}$	0.128	3.496	10^{-5}

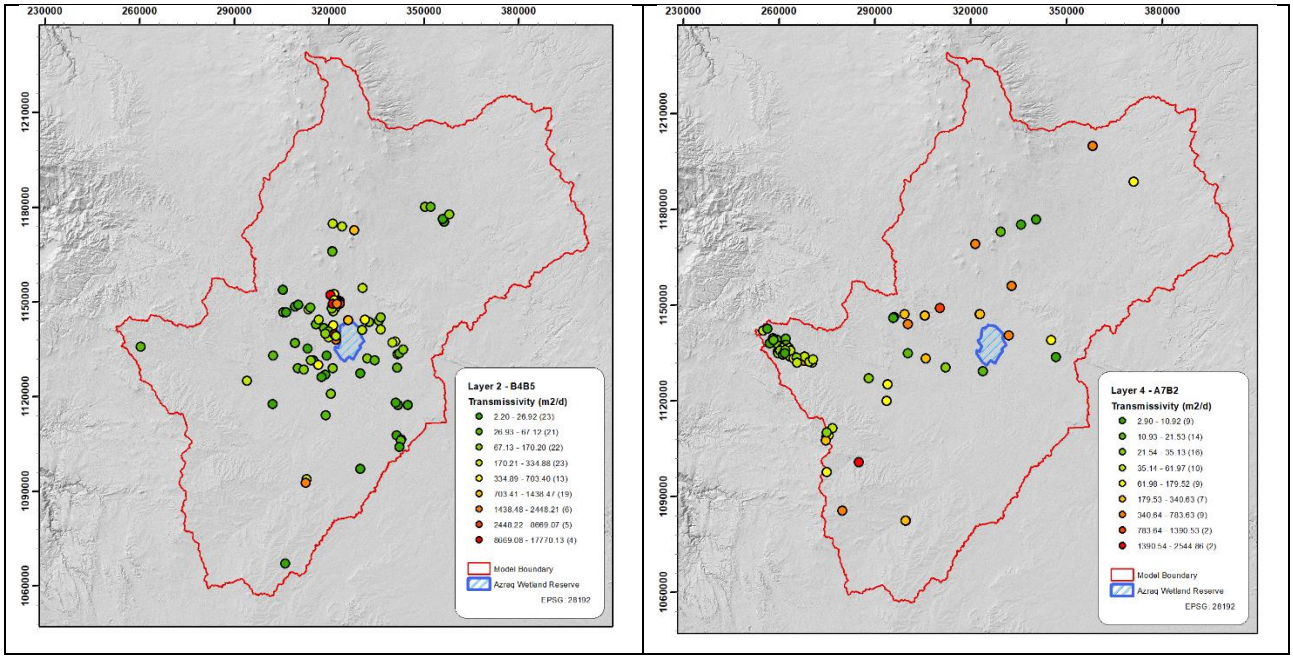

Figure 3-5. Transmissivity estimations for model layers 2 and 4 obtained from specific capacity data.

3.5 Sources and Sinks

In this section, the implementation of sources and sinks of groundwater in the flow model is described along with their respective stress rates, and how they are incorporated into the model.

3.5.1 Rainfall Infiltration

The recharge package of MODFLOW (RCH) was used to simulate the infiltration of rainfall into the subsurface of the Azraq Basin. Infiltration was applied to the uppermost active grid cell in each vertical column and was varied temporally for each stress period. Infiltration rates were assigned as a spatially heterogeneous distribution. The rates were assigned to the model as monthly averages for each stress period.

Infiltration was determined with a water balance approach that was applied to the Azraq Basin using GIS tools. The average annual infiltration rate for the model simulation period 2013-2020 was estimated at 89.68 Mm^3 per year. The methodology is outlined as collecting hydrological and hydrogeological information from different data sources, conducting statistical analyses of hydrological data for the different periods, analyzing meteorological data, and calculating the runoff rates. The water balance equation is used to calculate monthly water balances for the rainy season, which is defined for the period from September to March. Rainfall data were obtained as measurements at meteorological stations, whereas monthly runoff was estimated using runoff coefficients after the method by GTZ and NRA (1977). Runoff coefficient maps are used to estimate the infiltration rate as a fraction of rainfall depending on the topography and the soil types within the basin. Furthermore, potential evapotranspiration was computed with the Penman-Monteith method. Consequently, the water balance components were obtained for the model simulation period of Jan 2013 – Dec 2020.

The water balance equation used in the estimation is the following:

$$R = PPt - (E - FF) \qquad \text{(Equation 3)}$$

where:

R : Recharge
PPt : Precipitation
E : Evapotranspiration
FF : Flood flow

The kriging interpolation method was applied in GIS to produce final maps of each water budget component, followed by overlaying to obtain the recharge map. Fourteen rainfall stations are located in the basin of which, eleven stations are located in the Jordan side of the basin, and three stations are in Syria (Figure 3-6).

Table 3-3 summarizes rainfall data from the meteorological stations in the Azraq Basin. The highest monthly rainfall values were recorded in Salkhad (Syria), and the minimum monthly values were measured in the EI-Umary station, while Um El-Quttein rainfall station represents the average monthly values in the basin.

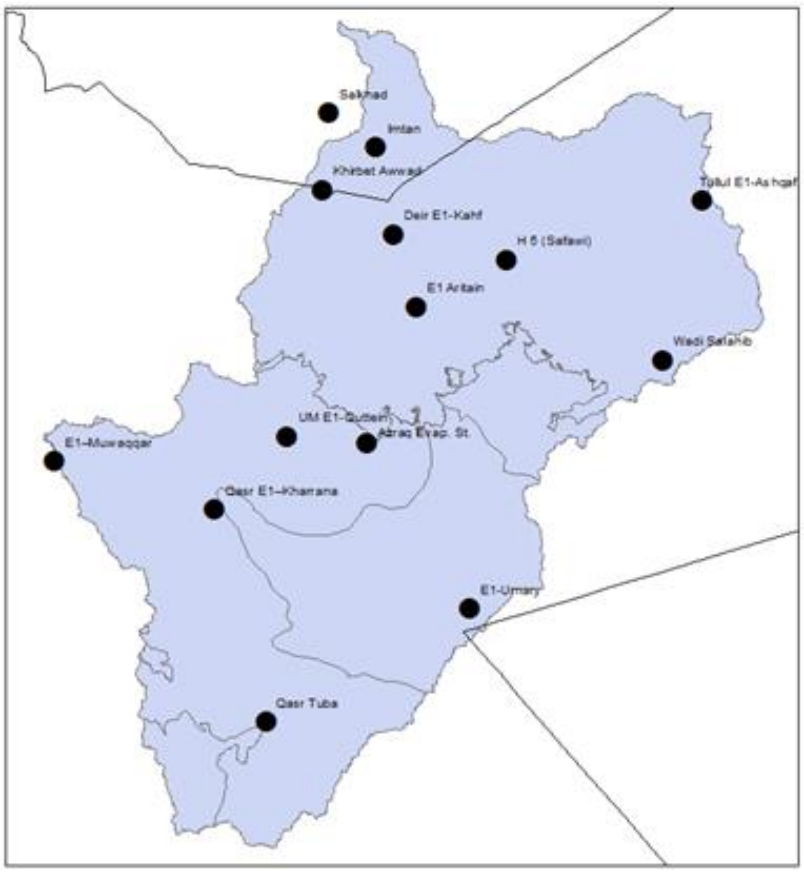

Figure 3-6. Meteorological stations used in the infiltration rate estimation for the Azraq Basin (WAJ, Open Data).

Table 3-3. Average rainfall records in the studied period (WAJ, Open Data).

Meteorological Station	Maximum Annual Rainfall (mm)	Minimum Annual Rainfall (mm)	Average Annual (mm)
Salkhad	533	163	325
Um El- Quttain	277	59	140
Safawi	189	15.5	66.5
Al-Aritain	170	39.5	91.7
Azraq Evap. Station	149	9.8	59
Qasr El-Kharrana	134	21	73
Qasr Touba	108	10	56
El- Mwaqqar	323	67	156
El-Umary	97	8.5	49
Tullul El- Asgqaf	121	15	68
Wadi Salahib	110	21.5	65
Deir Al-Kahf	168	36	108
Khirbit Awwad	368	76	199

Results are presented in Figure 3-7, Figure 3-8, and Figure 3-9. Lower annual recharge rates by more than 30% for the last 3 years of the study period were evident. It is clear that higher rainfall areas in the upper northern parts of Syria dominated the high infiltration rate of 170 mm/yr. Also, more than 50% of the basin area receives less than 100 mm/yr infiltration.

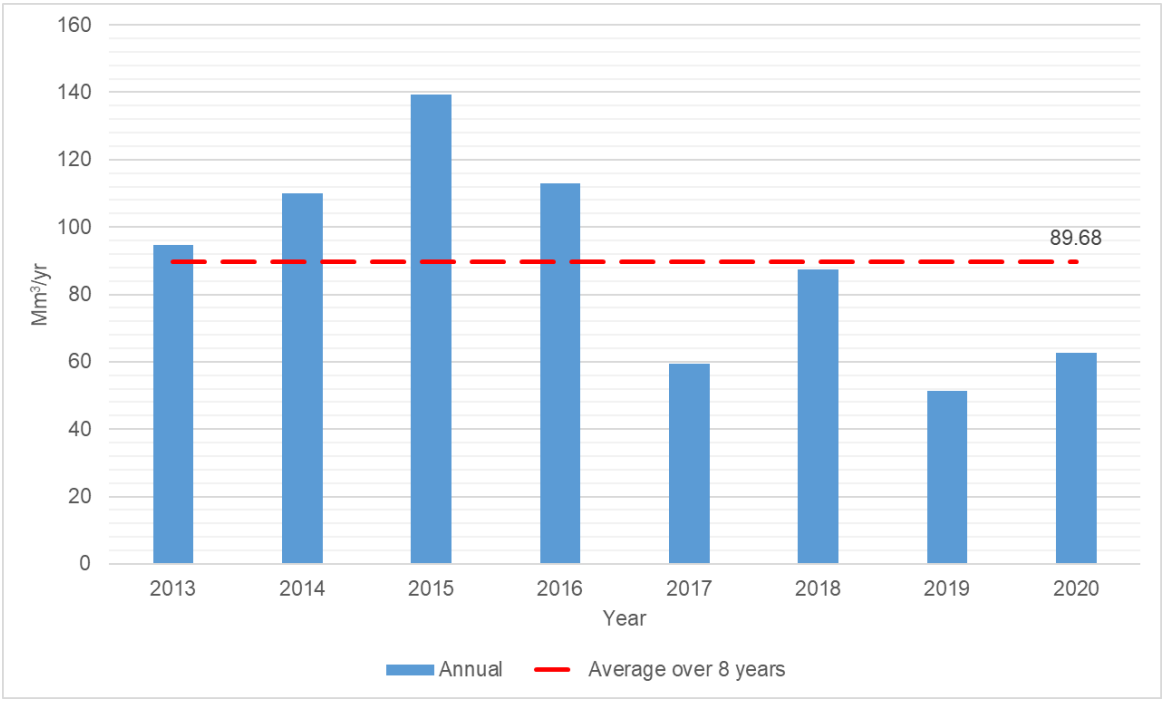

Figure 3-7. Basin-averaged annual infiltration rates estimated for input to the flow model.

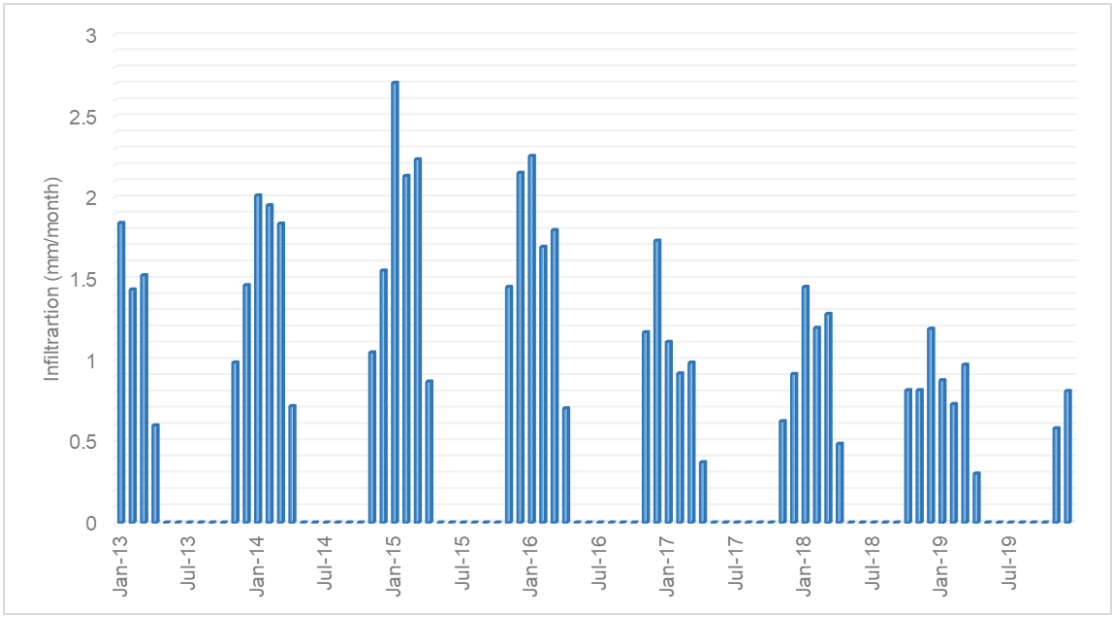

Figure 3-8. Basin-averaged monthly infiltration rates estimated for input to the flow model.

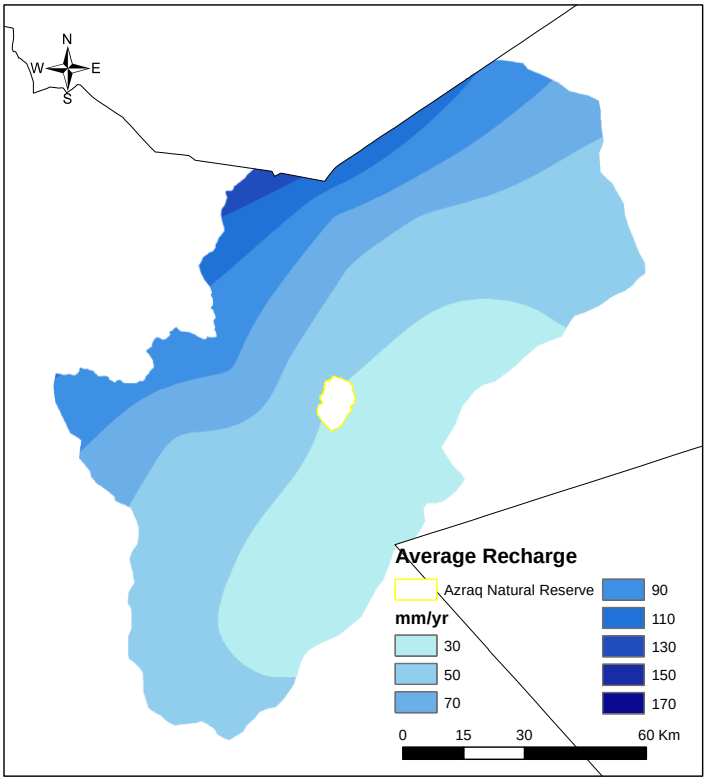

Figure 3-9. Annual average groundwater infiltration rate distribution in the Azraq Basin over the years 2013-2020.

3.5.2 Evapotranspiration

The evapotranspiration subroutine of MODFLOW (EVT) was implemented to account for the removal of groundwater from areas in the basin, 1) where the water table is relatively shallow, and 2) where vegetation in combination with high evaporation is expected to remove groundwater from the system. To this end, two ETP zones were defined in the model domain. The first ETP zone is the wetland catchment and the second zone is the remainder of the Azraq Basin. The parameter 'evapotranspiration rate' is the maximum evapotranspiration flux. A higher rate was assigned for the wetland zone. The parameter 'ETP depth' is the ETP extinction depth below which ETP ceases. Both parameters were handled as calibration parameters. Lastly, the third parameter 'ETP surface' defines the boundary above which the ETP flux is set to the maximum ETP rate. The top elevation of the model grid representing the ground surface is assigned as the ETP surface.

3.5.3 Extraction Wells

Extraction wells are the main sinks in the model, where groundwater is removed from the grid cell at a specified rate equal to the discharge rate of each well. Two types of pumping wells were distinguished in this study: irrigation wells and public water supply (PWS) wells that serve groundwater for domestic use. Depending on the well screen elevation pumping wells were assigned to withdraw groundwater from model layers 1, 2, and 4. The locations of the pumping wells are shown in Figure 3-10. All well coordinates are retrieved from a database. The database was obtained from the Groundwater Monitoring Unit of the Ministry of Water and Irrigation (MWI) in Jordan. Time series of monthly average discharge rates of the pumping wells were also provided in the database. Some properties of all defined wells in the model are provided in Table 3-4, and the resulting annual sums of groundwater discharge are given in Figure 3-11.

Table 3-4. Estimations of pumping rates for the wells assigned as model input data.

Well Type	Number of Wells	Average Annual Groundwater Pumping Rate (Mm^3/yr)	Range of Average Daily Pumping Rate (m^3/d)
Irrigation Wells	552	34.617	1.027 - 1268.93
Domestic Wells – AWSA	17	15.871	838.70 – 4621.07
Domestic Wells – Other	40	7.456	0.072 – 2276.69

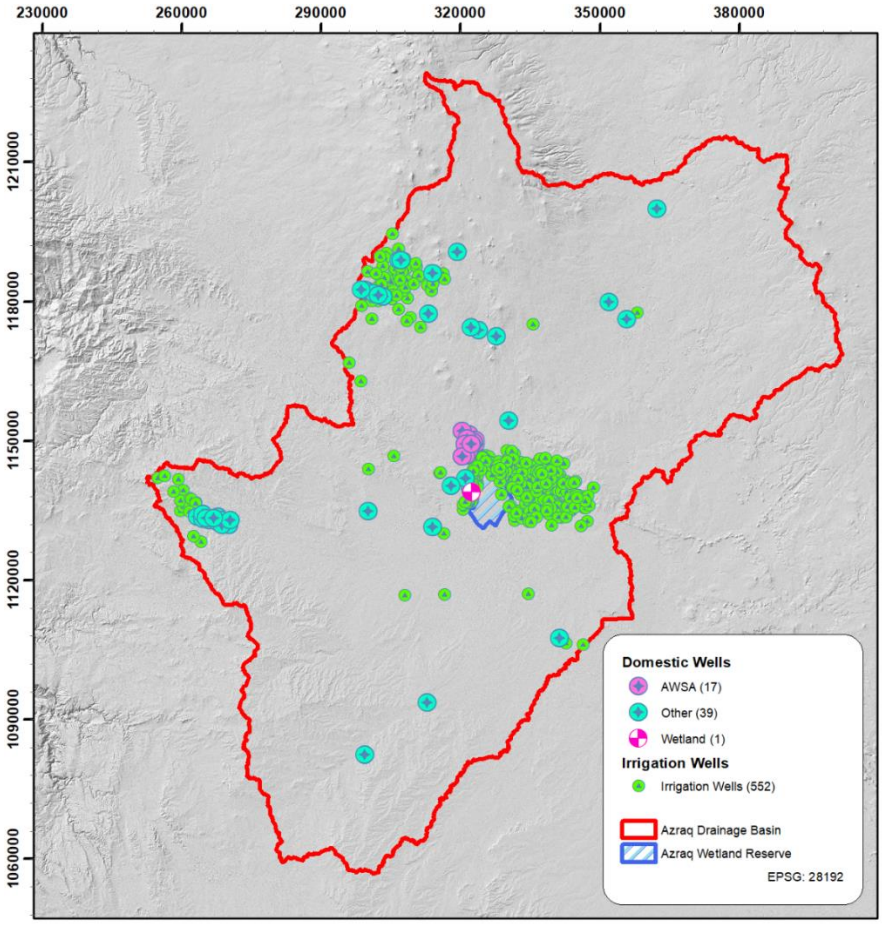

Figure 3-10. Location of pumping wells defined in the Azraq Basin flow model.

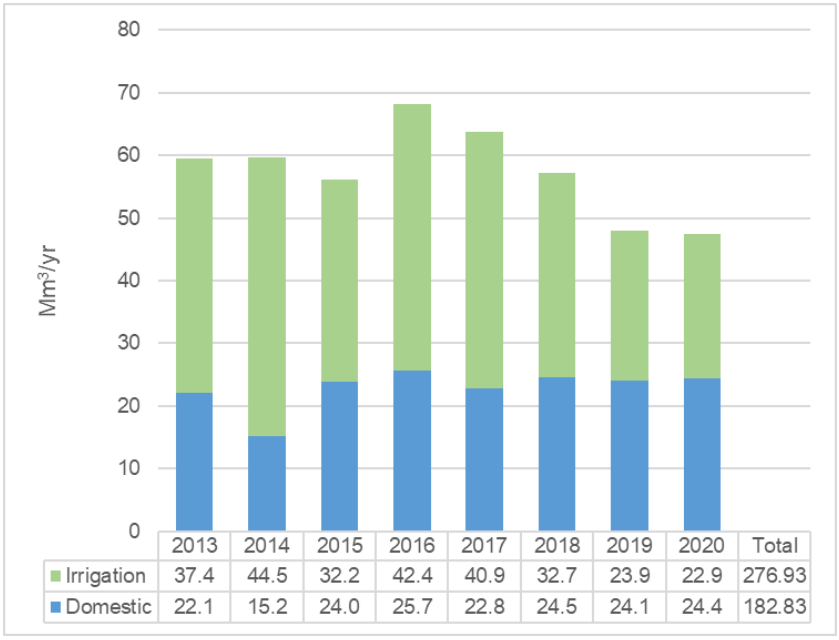

	2013	2014	2015	2016	2017	2018	2019	2020	Total
Irrigation	37.4	44.5	32.2	42.4	40.9	32.7	23.9	22.9	276.93
Domestic	22.1	15.2	24.0	25.7	22.8	24.5	24.1	24.4	182.83

Figure 3-11. Yearly pumping rates of extraction wells in the Azraq Basin that were assigned in the flow model.

3.6 Calibration Data

A data set of groundwater level measurements from 15 observation wells were obtained for the modeling study. Groundwater levels are monitored by the MWI in Jordan. The time span of measurements is available starting from the year 2005 until the end of 2020. The groundwater level data from these observation wells that are used in model calibration hereafter are referred to as calibration targets. All calibration targets are contained in the calibration dataset. Observations from 15 wells in the model domain and 421 observation records were used to create the calibration dataset (Table 3-5 and Figure 3-12). All observation records were screened for any potential outlier values, for example, observations that deviate significantly from previous and antecedent records.

Table 3-5. Selected head observation wells used in the calibration of the Azraq Basin flow model.

Well ID	Northing (m)	Easting (m)	Altitude(m)	Well Depth (m)	Number of Observations	Start Date	End Date
F1002	1130033	316420	523	38	3	Aug-2016	Jul-2017
F1014	1141030	330359	510	60	44	Jan-2013	Aug-2021
F1022	1141300	320376	520	88	35	Jan-2013	Aug-2021
F1043	1149404	322395	517	255	48	Feb-2013	Aug-2021
F1060	1140290	336710	521	116	21	Jan-2013	Jun-2015
F1063	1107619	341329	543	301	11	Mar-2014	May-2017
F1126	1132986	319138	514	146	33	Jan-2013	Aug-2021
F1145	1146675	305590	598	550	21	Feb-2013	Jun-2015
F1280	1147863	323783	514	195	25	Jan-2013	Oct-2015
F1286	1092613	312481	678	164	35	Jan-2013	Mar-2021
F1334	1180000	350300	710	366	51	Jan-2013	Aug-2021
F3222	1152143	320338	557	171	15	Feb-2013	Jun-2015
F3755	1134400	261100	805	527	26	Jan-2013	Jan-2016
F3979	1149100	310150	558	100	29	Jan-2013	May-2017
F4120	1146875	302027	637	161	24	Jan-2013	Aug-2020

Table 3-6. Statistical properties of groundwater levels in selected calibration dataset.

Well ID	Number of Observations	Minimum (m)	Mean (m)	Maximum (m)	Std. Deviation (m)	Trend in Groundwater Level
F1002	3	508.8	509.1	509.3	0.20	indistinct
F1014	44	478.3	485.1	491.0	3.06	decreasing
F1022	35	479.5	486.2	490.1	3.06	decreasing
F1043	48	477.0	485.1	490.0	3.48	decreasing
F1060	21	490.3	492.0	494.9	1.46	decreasing
F1063	11	521.3	522.5	523.1	0.42	indistinct
F1126	33	502.2	502.8	503.0	0.17	decreasing

Well ID	Number of Observations	Minimum (m)	Mean (m)	Maximum (m)	Std. Deviation (m)	Trend in Groundwater Level
F1145	21	508.1	509.2	511.8	1.12	decreasing
F1280	25	484.9	488.2	491.7	1.40	decreasing
F1286	35	554.6	555.4	555.7	0.25	decreasing
F1334	51	531.2	532.6	539.7	2.51	increasing
F3222	15	491.1	492.2	493.5	0.66	indistinct
F3755	26	478.8	480.1	482.0	0.83	indistinct
F3979	29	501.6	503.4	504.8	0.77	decreasing
F4120	24	503.0	503.4	503.8	0.19	decreasing

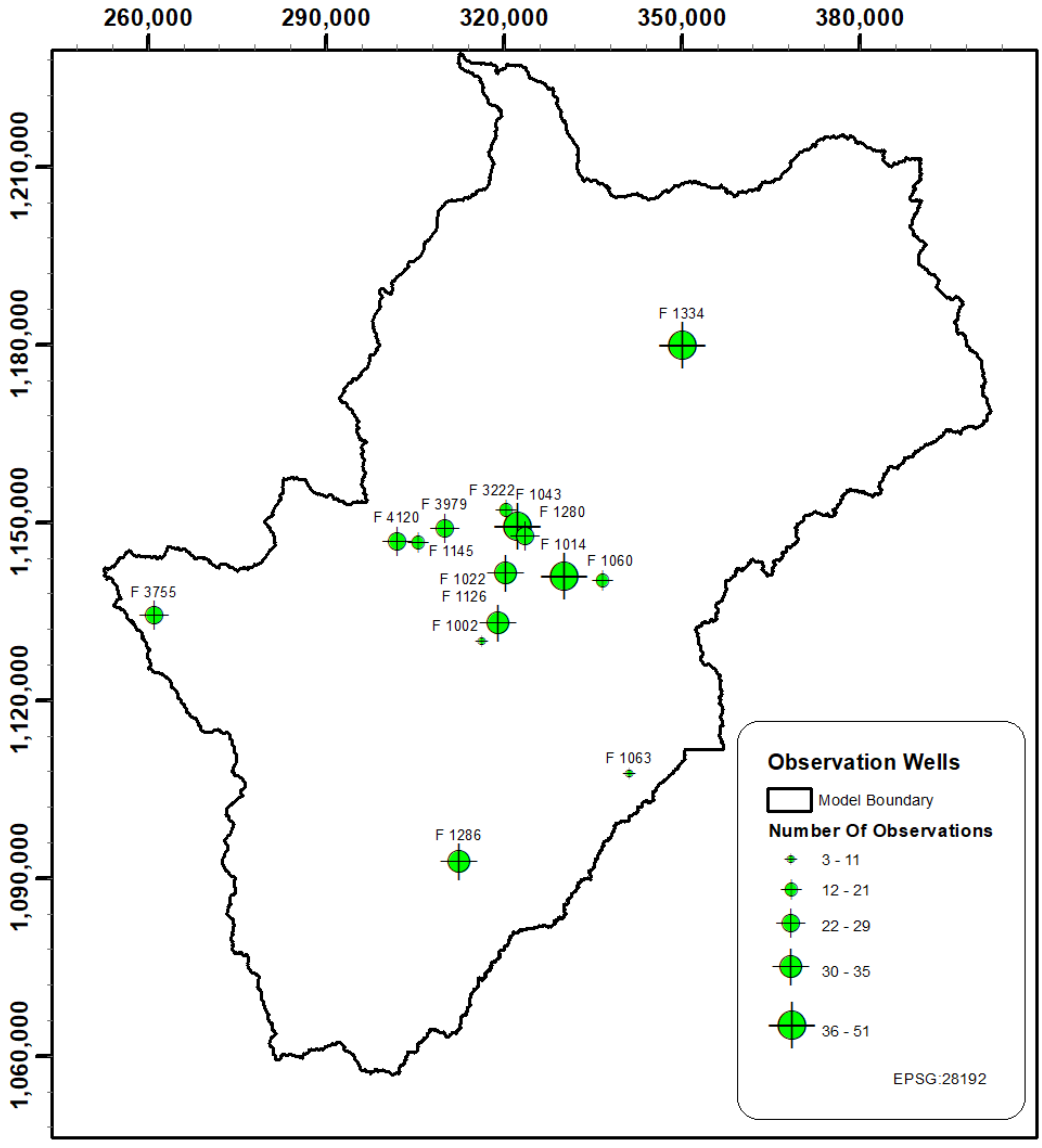

Figure 3-12. Locations of observation wells used in the model calibration and number of measurements available for each well.

3.7 Numerical Solver Settings

The finite-difference flow equations were numerically solved by the Preconditioned Conjugate-Gradient method (Harbaugh, 2005). The selection of numerical parameters used in the solution method is summarized in Table 3-7.

Table 3-7. Parameters of the Preconditioned Conjugate-Gradient (PCG) package that is used to solve the finite difference equations in each step of a MODFLOW stress period.

Max number of outer iterations	20
Max number of inner iterations	30
Matrix preconditioning method	modified incomplete Cholesky
Max. abs change in head	0.005
Max abs residual	0.005
Relaxation parameter	1
Damping factor	1
Transient damping factor	1

4. MODEL CALIBRATION

This section of the deliverable describes calibration procedures, presents optimal parameter estimates, and a comparison of calibration targets to model-calculated hydraulic head values.

4.1 Calibration Procedure

Calibration is the process in which the model parameters are adjusted to improve the accuracy of the model and to demonstrate that the model is reasonably representative of observed site conditions. Calibration of the groundwater flow model was accomplished by systematically perturbating model parameters and matching groundwater levels measured between January 2013 and December 2020 with the simulated hydraulic heads.

Model calibration was performed in two phases; in the first phase, the model was calibrated manually (also called the trial-and-error method), which is the process of systematically changing model parameters, running the model with the changed input, and then comparing the result of the calibration with the calibration targets. The process is repeated until the simulated values compare favorably with the observed values. To evaluate calibration results and model accuracy quantitatively, the mean error (ME), mean absolute error (MAE), and root mean squared error (RMSE) were calculated for all calibration targets. Hydraulic heads calculated by the model were read from the model output file and evaluated using the Head Observation Package (HOB) (Hill et al., 2000).

The RMS error was calculated as:

$$RMSE = \sqrt{\frac{1}{n}\sum_{i=1}^{n}(h_m - h_s)_i^2} \qquad \text{(Equation 4)}$$

where

n is the number of residuals
h_m is the observed groundwater level at observation well i
h_s is the simulated hydraulic head at observation well i

The overall model accuracy is increased by minimizing the RMSE. However, the goal of the manual calibration was first to obtain a reasonable model solution that can be used as a starting point for automated calibration. Therefore, the goal was first to minimize ME values for each calibration target as much as possible, which implies matching the averages of observed and simulated values. In the second calibration phase, the manually pre-calibrated model was subject to automated calibration, which resembles manual calibration except that a computer code rather than the user adjusts the model parameters. Here the goal is to minimize a composite objective function that is based on a combination of model errors (residuals).

The flow model was calibrated by using the PEST parameter estimation computer code (Doherty, 2016). The automatic model calibration, with PEST, completes a single model simulation using a user-defined set of input parameters and compares model outputs to the calibration dataset. Subsequent model runs were performed with small changes in model parameters, and the model outputs are compared again with the calibration

dataset. The PEST code mathematically determines which input parameters to adjust to facilitate effective model calibration. It continued the process until an optimal set of model parameters was obtained, which provides the statistically best fit between model outputs and the calibration dataset. The PEST code implemented the Gauss-Levenberg-Marquardt algorithm. This algorithm is a gradient-based search method that adjusts parameters by attempting to minimize the sum of the squared and weighted residuals.

The implementation of Tikhonov regularization and the use of pilot points for the estimation of spatial hydraulic properties using PEST allows for a large number of model parameters to be optimized and estimated simultaneously. Regularization is the name given to a broad class of mathematical techniques that can be used to bring numerical stability to an otherwise over-parameterized inverse problem through the introduction of an appropriate smoothness or other constraints on parameter values (Tikhonov 1963a, 1963b; Barbosa and Silva, 1994). Using regularization in conjunction with pilot points is advantageous because many more parameters can be estimated compared to the number of observations used for calibration (Doherty, 2003). The method of pilot points (Doherty, 2003) was used to interpolate a hydraulic conductivity field for each layer of the model, and apply the resulting spatially variable distribution of hydraulic conductivity to the model grid.

4.2 Calibration Parameters

Calibration parameters were defined to represent hydraulic properties and various settings of the evapotranspiration head-dependent boundary conditions of the model. Parameters adjusted during model calibration were horizontal hydraulic conductivity, vertical anisotropy ratio, storage coefficient of Layers 2, 3, and 4, specific yield of Layer 1, maximum ETP rate, and the extinction depth of ETP. A total of 12 calibration parameters in 3 parameter groups were defined in the PEST calibration setup.

The horizontal hydraulic conductivity distributions in Layers 2 and 4 were estimated with kriging interpolation of 180 pilot points by using the initial K distribution as prior information. Pilot points are user-defined locations distributed in and around the model domain that represent surrogate parameters from which hydraulic conductivity values are interpolated to the model grid. The horizontal hydraulic conductivity fields of each model layer were adjusted during the automatic calibration using multipliers. The use of the pilot point approach allowed a reasonable representation of regional heterogeneity. Similarly, the storage coefficients of Layers 2 and 4 were adjusted with the pilot point approach. Layers with homogeneous parameters were assigned multipliers as calibration parameters. Parameters related to ETP were directly handled as calibration parameters. Ranges of plausible parameter values were identified for all calibration parameters (Table 4-1), which were implemented as lower and upper parameter limits in PEST.

Table 4-1. Calibration parameters and parameter value bounds.

Parameter Name	Parameter Description	Parameter Group	Lower Bound	Upper Bound	Units
EVT_Dep_C	Evapotranspiration Extinction Depth inside wetland catchment	EVPs	5	30	m
EVT_Depth	Evapotranspiration Extinction Depth outside wetland catchment	EVPs	5	60	m
EVT_Rate	Evapotranspiration Rate	EVPs	2.5E-03	0.01	m/d
K_A7B2	Horizontal Hydraulic Conductivity of A7B2 Aquifer	HKs	0.0114	69.93	m/d
K_B3	Horizontal Hydraulic Conductivity of B3 Aquitard	HKs	1E-04	1	m/d
K_B4B5	Horizontal Hydraulic Conductivity of B4B5 Aquifer	HKs	4.5E-03	280.6	m/d
K_Basalt	Horizontal Hydraulic Conductivity of Basalt Aquifer	HKs	0.3	50	m/d
m_VK_All	Vertical Anisotropy Ratio (HK/VK)	HKs	1	100	-
Ss_A7B2	Specific Storage of A7B2 Aquifer	SSs	8E-07	2E-04	m^{-1}
Ss_B3	Specific Storage of B3 Aquitard	SSs	8E-07	2E-04	m^{-1}
Ss_B4B5	Specific Yield of B4B5 Aquifer	SSs	2.3E-06	0.15	m^{-1}
Sy_Basalt	Specific Yield of Basalt Aquifer	SSs	0.001	0.1	-

4.3 Sensitivity Analysis

A sensitivity analysis was performed to determine which parameters are effective on the model results. This analysis was conducted on the parameters listed in Table 4-1. The one-at-a-time perturbation approach was used, where independence among tested parameters is assumed. Each parameter was changed one at a time by ±50 % of its initial value and changes in the RMSE of the simulated head were noted. A sensitivity statistic, S, (Equation 4) was calculated such that when for example a 10% change in the parameter value results in a 10% change in the model result, the sensitivity statistic yields 1.00.

$$S = \frac{RMSE_{pos} - RMSE_{neg}}{2 \cdot RMSE_{baseline}} \cdot \frac{p}{\Delta p} \qquad \text{(Equation 5)}$$

where:

S: sensitivity statistic
p: baseline parameter value
Δp: perturbation range of parameter
$RMSE_{pos}$: RMSE after a positive change in the parameter value
$RMSE_{neg}$: RMSE after a negative change in the parameter value
$RMSE_{baseline}$: baseline RMSE

Analysis results shown in Table 4-2 suggested that the model is most sensitive to EVT_Dep_C (evapotranspiration extinction depth inside wetland catchment). Other sensitive parameters, in the order of decreasing sensitivity, were the maximum rate of evapotranspiration, the specific storage coefficient of Layer 2, and the hydraulic conductivity of Layer 2.

Table 4-2. Sensitivity analysis results.

Parameter Name	$RMSE_{neg}$	$RMSE_{pos}$	Sensitivity Statistic, S
EVT_Dep_C	5.47815	16.36926	0.538307
EVT_Rate	6.16648	7.277469	0.054912
HK_Basalt	6.73116	6.775702	0.002202
SY_Basalt	6.74135	6.772708	0.000235
EVT_Depth	6.74383	6.747117	0.000162
SS_B3	6.76332	6.705057	-0.00044
SS_A7B2	6.78855	6.537302	-0.00188
HK_A7B2	6.77105	6.673165	-0.00484
HK_B3	6.78621	6.683054	-0.0051
HK_B4B5	6.85725	6.666765	-0.00942
SS_B4B5	7.73019	5.577879	-0.01612

4.4 Calibration and Parameter Estimation Results

Calibration results are presented here as a report of model parameter estimates, and comparisons of calibration targets to model-calculated hydraulic head values. The optimal ranges of parameter values and median calibrated parameter values in the case of heterogeneous layers are presented in Table 4-3. Final parameters of pilot points are not shown here. The final calibrated parameter distributions over the model domain were obtained as a result of model calibration. The interpolated hydraulic conductivity fields for all model layers are presented in Figure 4-1. The calibrated storage coefficient fields are shown in Figure 4-2. Pilot points are also shown for the layers for which they were used.

Table 4-3. Starting and final values of calibration parameters (median values are given for heterogeneous layers).

Calibration parameter name	Applicable Model Layer	Starting Value (median)	Calibrated value (median)	Units
EVT_Dep_C	L1 or L2	16.964	7.272	m
EVT_Depth	L1 or L2	10.643	23.335	m
EVT_Rate	L1 or L2	0.004	0.01	m/d
K_A7B2	L4	0.074 -56.4 (2.062)	0.011 - 8.75 (0.320)	m/d
K_B3	L3	2.96E-03	2.68E-03	m/d
K_B4B5	L2	0.022 – 135.1 (1.362)	0.004 - 42.88 (0.588)	m/d
K_Basalt	L1	7.344	11.83	m/d
m_VK_All	L1-L2-L3-L4	8.62	1.03	-
Ss_A7B2	L4	1E-04	7.8E-07 - 2E-04 (9.8E-06)	m^{-1}
Ss_B3	L3	1E-04	7E-06	m^{-1}
Ss_B4B5	L2	6.90E-06 - 0.008 (4.72E-05)	3.25E-06 - 0.004 (3.25E-05)	m^{-1}
Sy_Basalt	L1	0.002	0.011	-

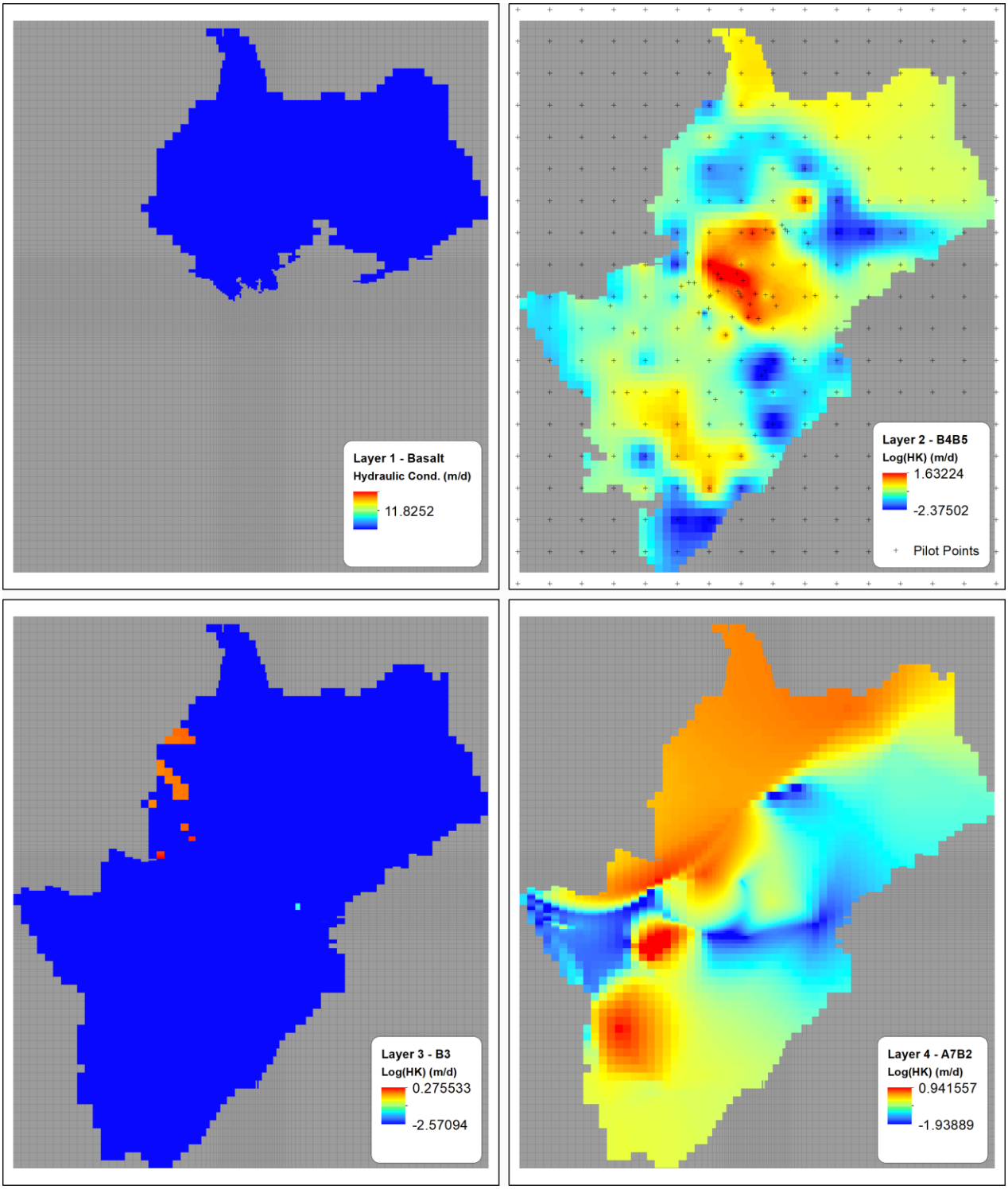

Figure 4-1. Calibrated horizontal hydraulic conductivity ($K_x = K_y$) distribution.

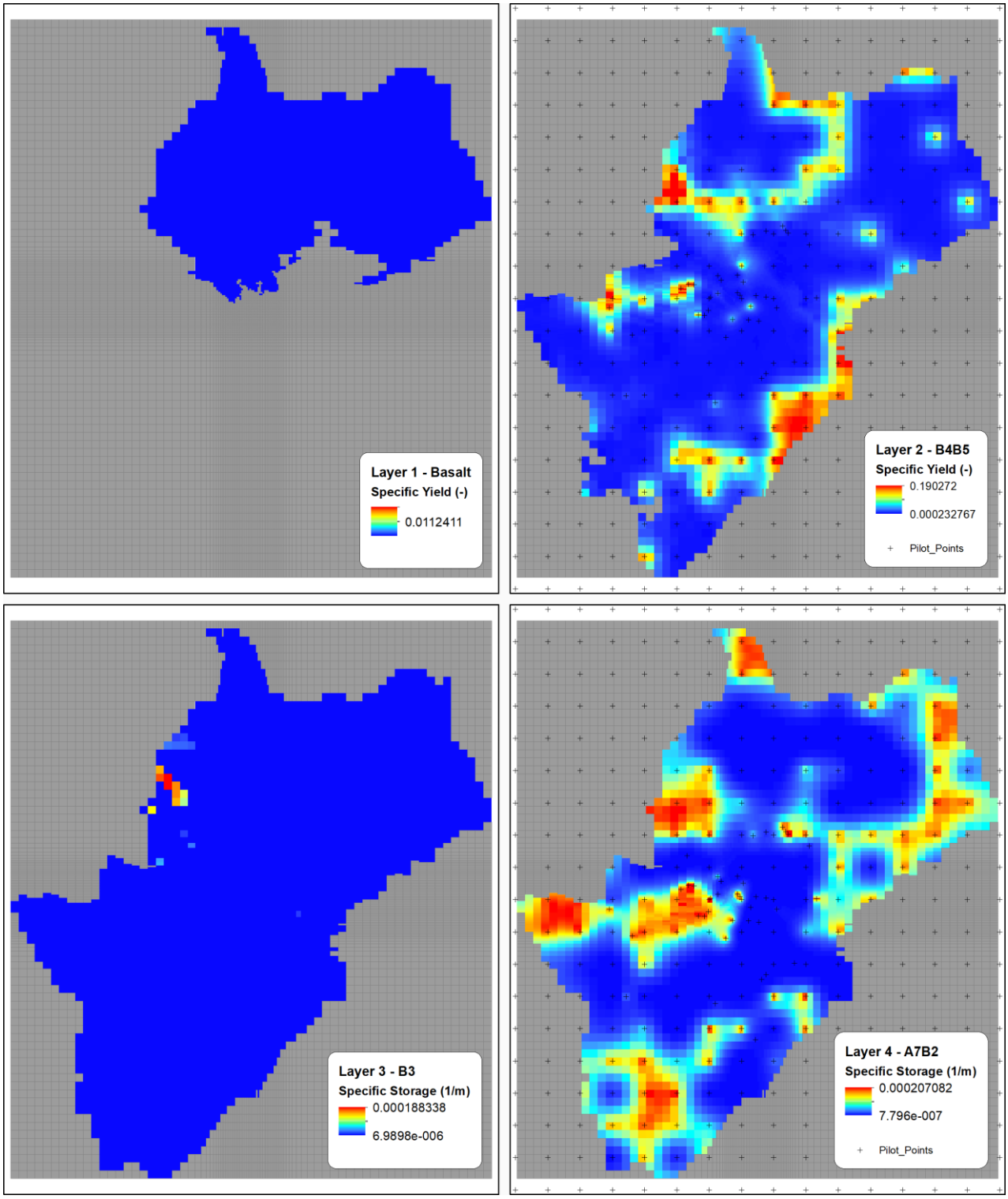

Figure 4-2. Calibrated specific storage distribution.

The 421 hydraulic head calibration targets for wells in the Azraq Basin were compared with model-calculated hydraulic heads at the same location and time as the observations. Using all calibration targets from 15 observation wells, the RMS error was 2.14 m, and the mean of absolute errors (MAE) was 1.51 m. The median absolute error was also determined as it is less affected by data outliers. The median absolute error was determined as 1.11 m, which is satisfactory given the range and order of magnitude of observed groundwater levels.

The average head residuals for each observation well were determined by calculating the average of all residuals in time for the well. Positive average hydraulic head residuals (observed minus simulated values), which indicate an underestimation of the model, varied in magnitude without any obvious pattern in their spatial distribution (Figure 4-3). Average head residuals were within the range of -0.76 – 4.16 m. The negative residuals were detected near the wetland boundaries at wells F-1014 and F-1022. Also, the largest positive residual was seen at well F-1145, which is located farther away from the wetland area but within the boundaries of the wetland catchment.

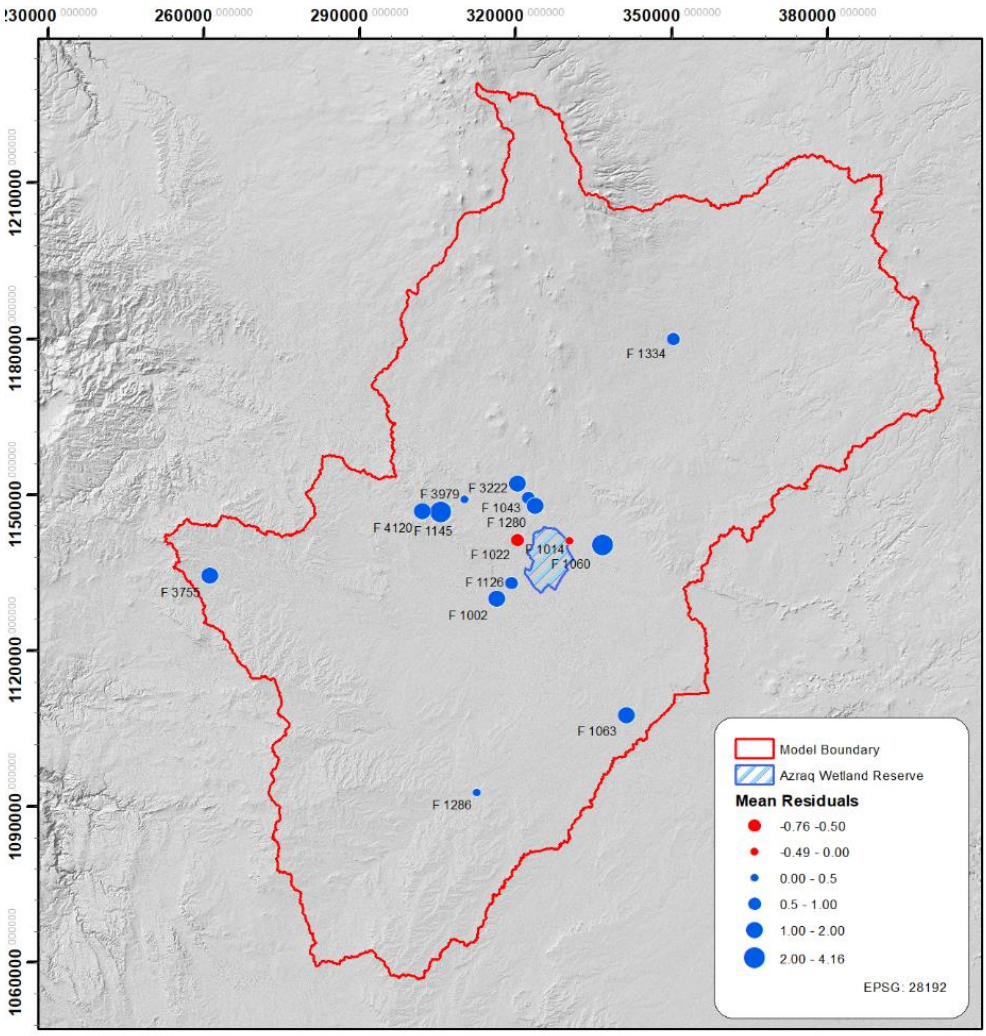

Figure 4-3. Temporally averaged head residuals (observed minus simulated values) of hydraulic head calibration targets.

Observed hydraulic head values were plotted against simulated values and compared to a 1:1 perfect-fit line (Figure 4-4). Overall, the scatter of data points was spread equally above and below the 1:1 line, suggesting that simulated hydraulic heads were generally close to observed data, and simulated heads were evenly balanced around the calibration targets. Hydraulic head residuals, i.e. the observed head minus the simulated head, are shown in a histogram to assess the overall model fit to observations. It is evident from the histogram that residuals were near to normally distributed around zero, which indicates a random distribution of model errors without any systematic error in the model (Figure 4-5). The number of positive residuals was larger than the negative residuals suggesting that the model was slightly biased toward underestimation of hydraulic heads. This could be confirmed also by the mean error of ME = 0.94 m.

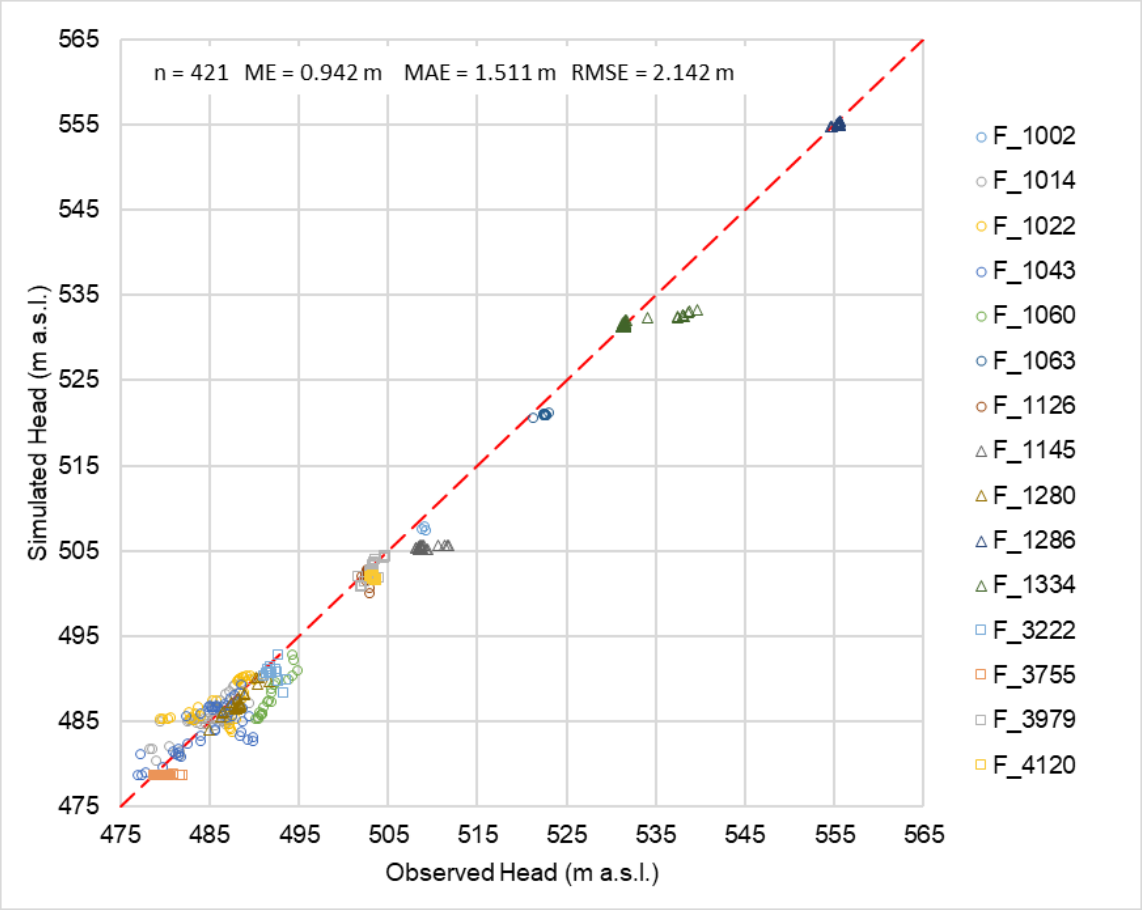

Figure 4-4. Comparison of observed and simulated hydraulic heads (r^2=0.998) for calibration targets showing a 1:1 perfect-fit line for reference.

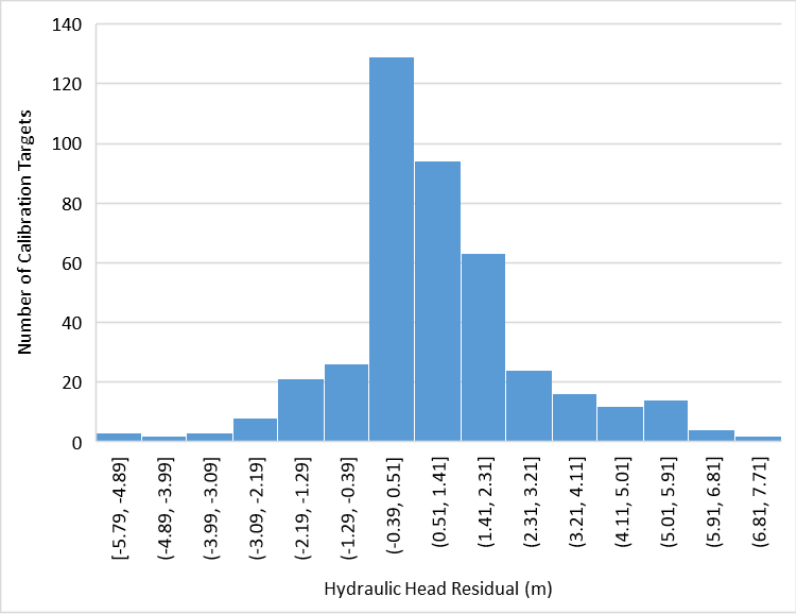

Figure 4-5. Histogram of hydraulic head residuals for the Azraq Basin flow model.

5. MODEL RESULTS

In this section, the outcomes of the groundwater flow simulation with the calibrated model for the Azraq Basin are presented. Results were analyzed in three parts; the analysis of groundwater flow for the entire basin is provided in the first part; in the second part modeling results pertaining to the Azraq Wetland Reserve are analyzed; the third part presents the modeling results related to the groundwater budget. Although it is possible to post-process model results in many different ways, the analysis of model results in this deliverable is limited to the mapping of simulated groundwater levels, plotting hydrographs, and processing of groundwater budget model outputs.

5.1 Simulated Groundwater Levels in the Azraq Basin

Simulated hydraulic head distribution (potentiometric surface) and groundwater flow directions at the end of the simulation period (December 2020) are illustrated in Figure 5-1. Here it was evident that groundwater flow in the basin converges towards the center of the basin where the AWR is situated. Groundwater flow directions were variable over the whole model domain, predominantly flowing from the south to the north in the southern part of the basin. The lowest hydraulic heads were observed in the depression zone around the AWR in Layer 4 at 458.5 m. The highest groundwater levels could be observed mostly near the boundaries of the Azraq Basin, with a maximum head value of 617 m.

The difference in groundwater levels over the 8-year simulation period was analyzed to identify areas in the domain, where groundwater exploitation causes critical groundwater level declines. Groundwater levels, whether they are rising or declining, also represent changes in the aquifer groundwater storage. Figure 5-2 depicts the simulated drawdown in the potentiometric surface for all layers from January 2013 to the end of the simulation period (December 2020). At the end of the 8 years, groundwater levels declined up to 20.0 m near the AWR in the center of the basin.

Hydrographs of observed and simulated hydraulic heads illustrate the temporal changes in groundwater levels at selected observation locations in the Azraq Basin (Figure 5-3). Observation well locations can be looked up in Figure 3-12. A visual assessment of these hydrographs indicated that, overall, the fit between flow model hydrographs and observations is acceptable. The fit can be considered satisfactory in particular for wells F-1043, F-1280, F-3222, and F-3979.

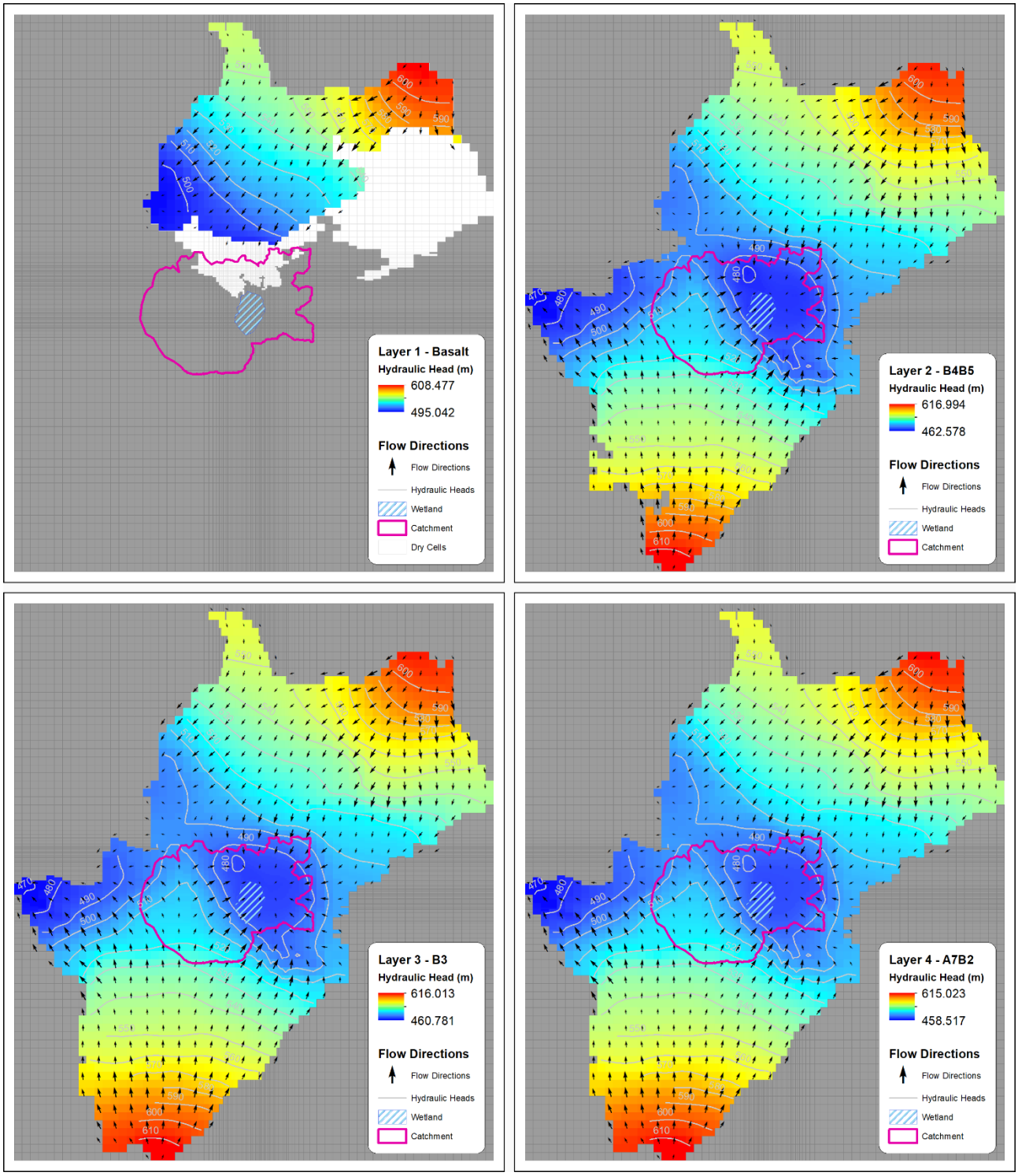

Figure 5-1. Hydraulic head distribution and groundwater flow direction in all model layers representing the end of the simulation period (December 2020).

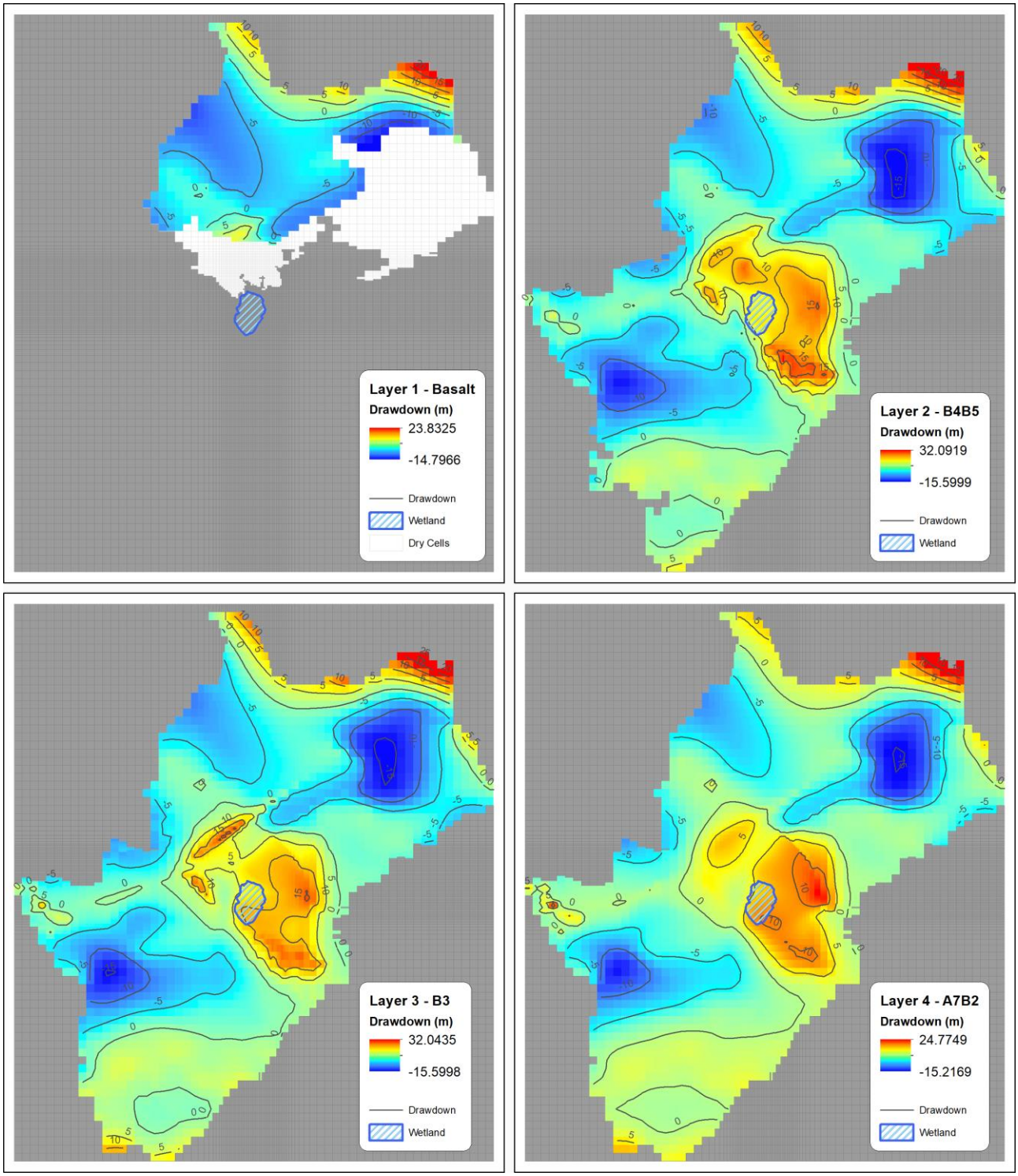

Figure 5-2. Simulated groundwater drawdown in all model layers since the beginning of the simulation (Jan 2013). Positive numbers indicate a decline, negative numbers indicate a rise in groundwater levels.

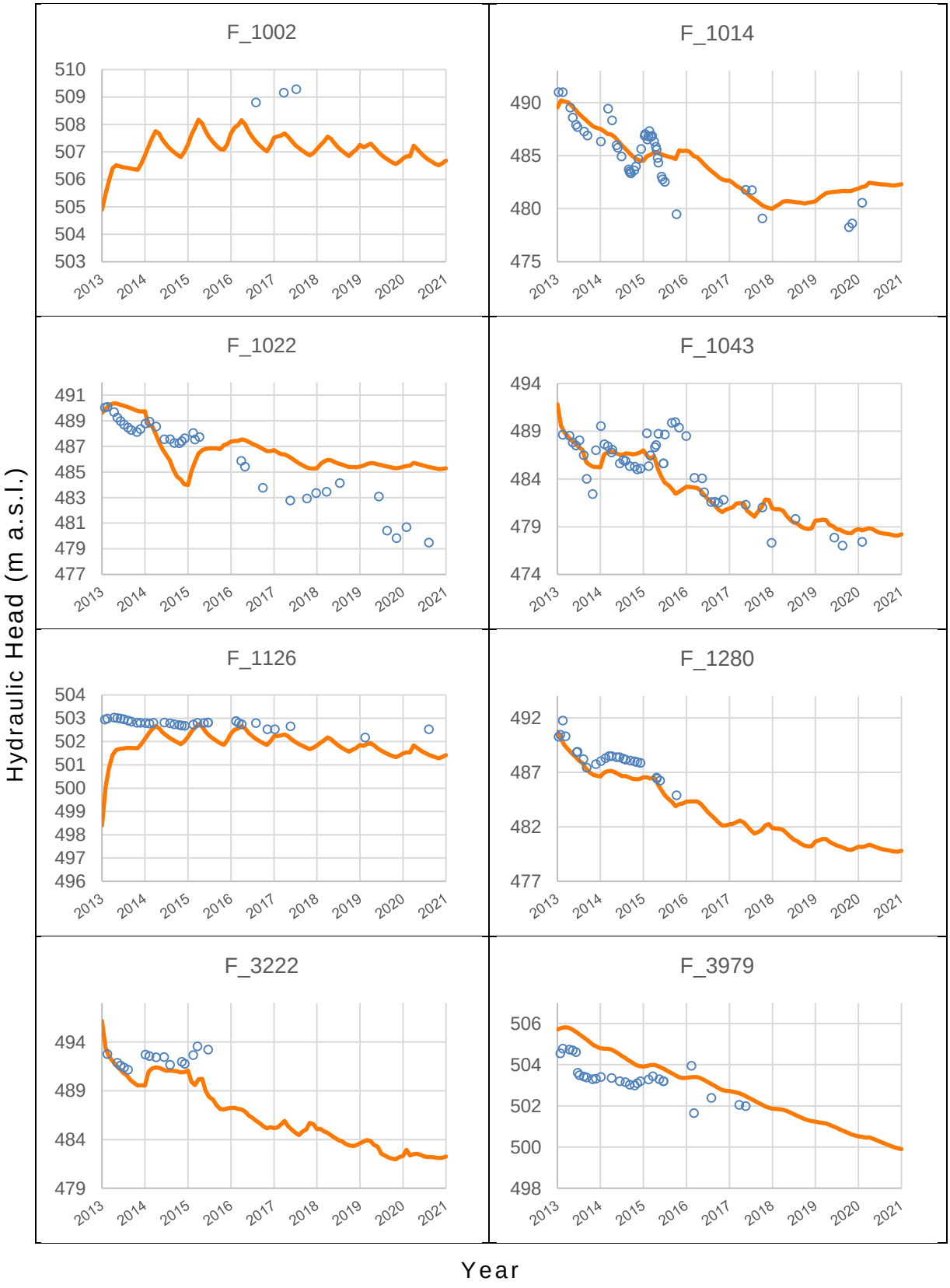

Figure 5-3. Hydrographs of observed and simulated heads for selected observation wells in the Azraq Basin.

5.2 Simulated Groundwater Flow in the Azraq Wetland Reserve

The solutions for the hydraulic head representing groundwater flow conditions in the wet and dry seasons in the vicinity of the AWR are depicted in

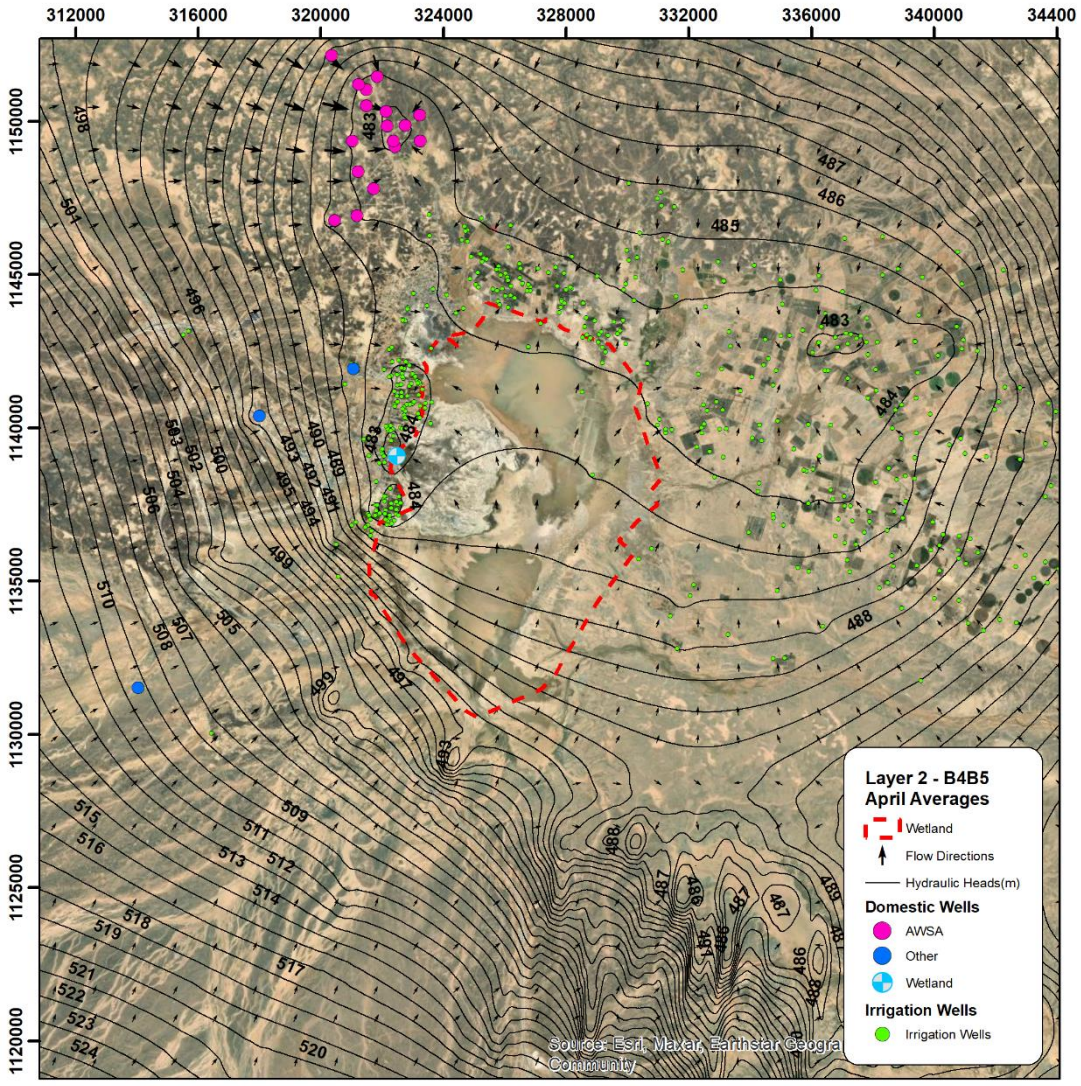

Figure 5-4 and Figure 5-5, respectively. In general, groundwater flowed towards the wetland area with steep hydraulic gradients in the west and the south. A depression zone formed about 4 km east of the wetland, in an area where irrigation wells are concentrated. The effect of evapotranspiration on the head pattern is visible in the southeast corner of the map.

Furthermore, the seasonal difference in groundwater levels in and around the AWR is shown in

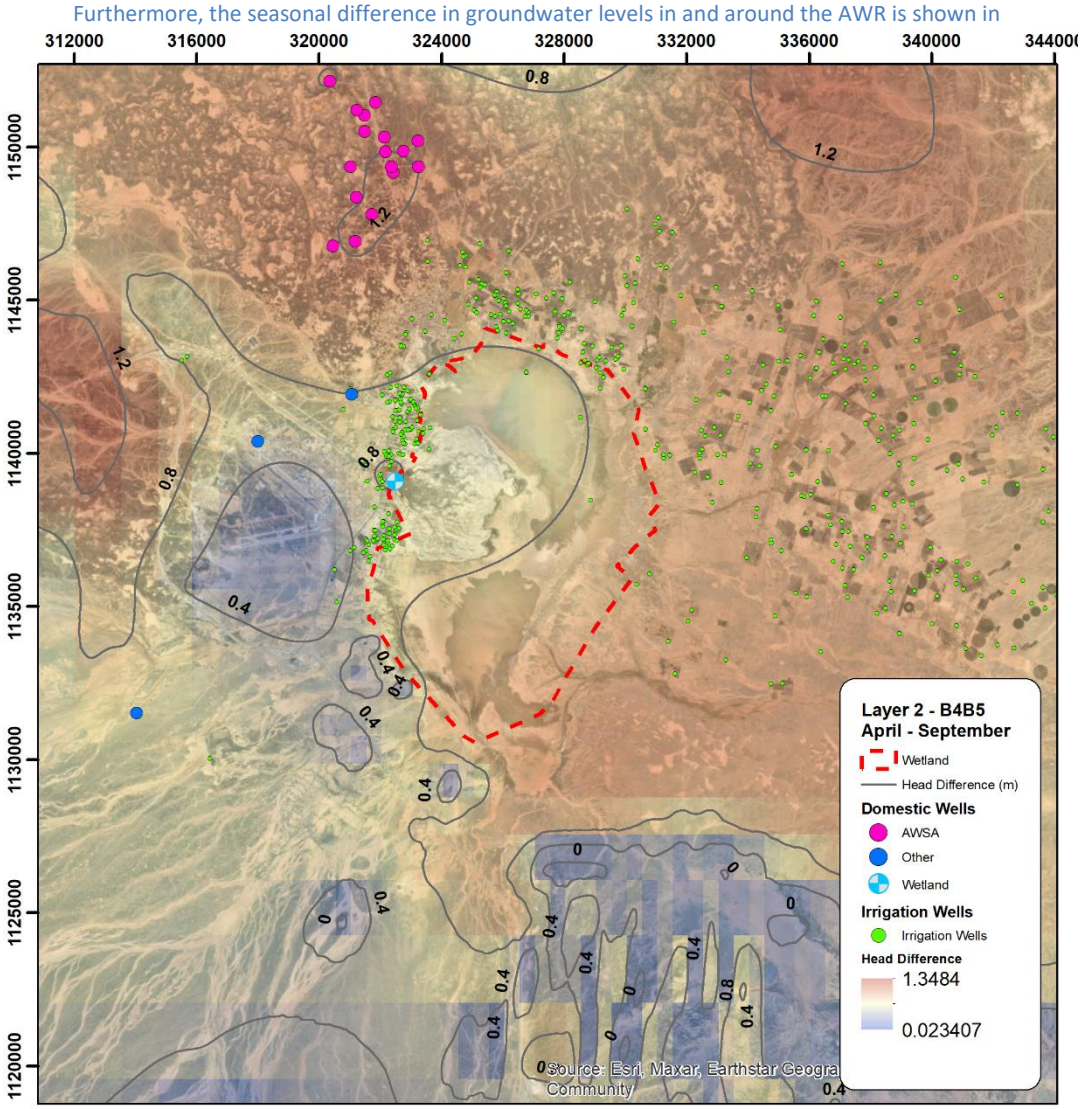

Figure 5-6. According to model results, average groundwater levels in September were lower than levels in April. The maximum difference in level was about 1.3 m which was observed outside the AWR. Within the boundaries of the AWR, the average seasonal decline in groundwater levels is about 0.8 m.

Vertical groundwater flow directions in the AWR are shown in Figure 5-7 and Figure 5-8. It is evident that groundwater predominantly flows upward thereby creating seepage to the wetland area although the seepage rate could be negligible to small vertical hydraulic gradients. Also, the simulated water table was below the ground surface at an average depth of about 22 m. This finding is consistent with data reported in the Azraq

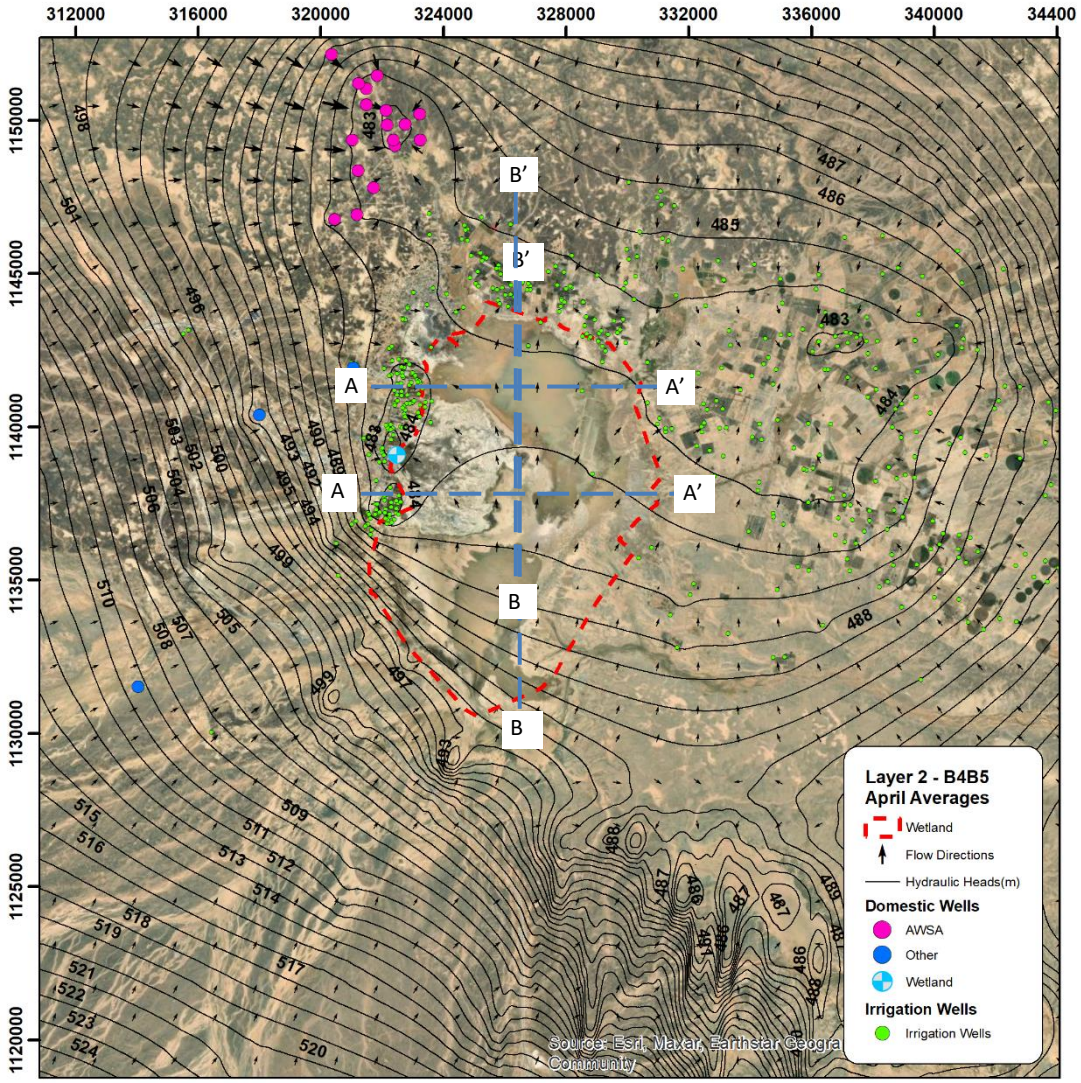

Figure 5-4. Temporally averaged hydraulic head distribution in Layer 2 calculated from model solutions of the month of April.

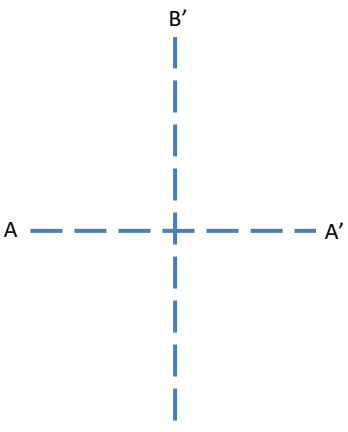

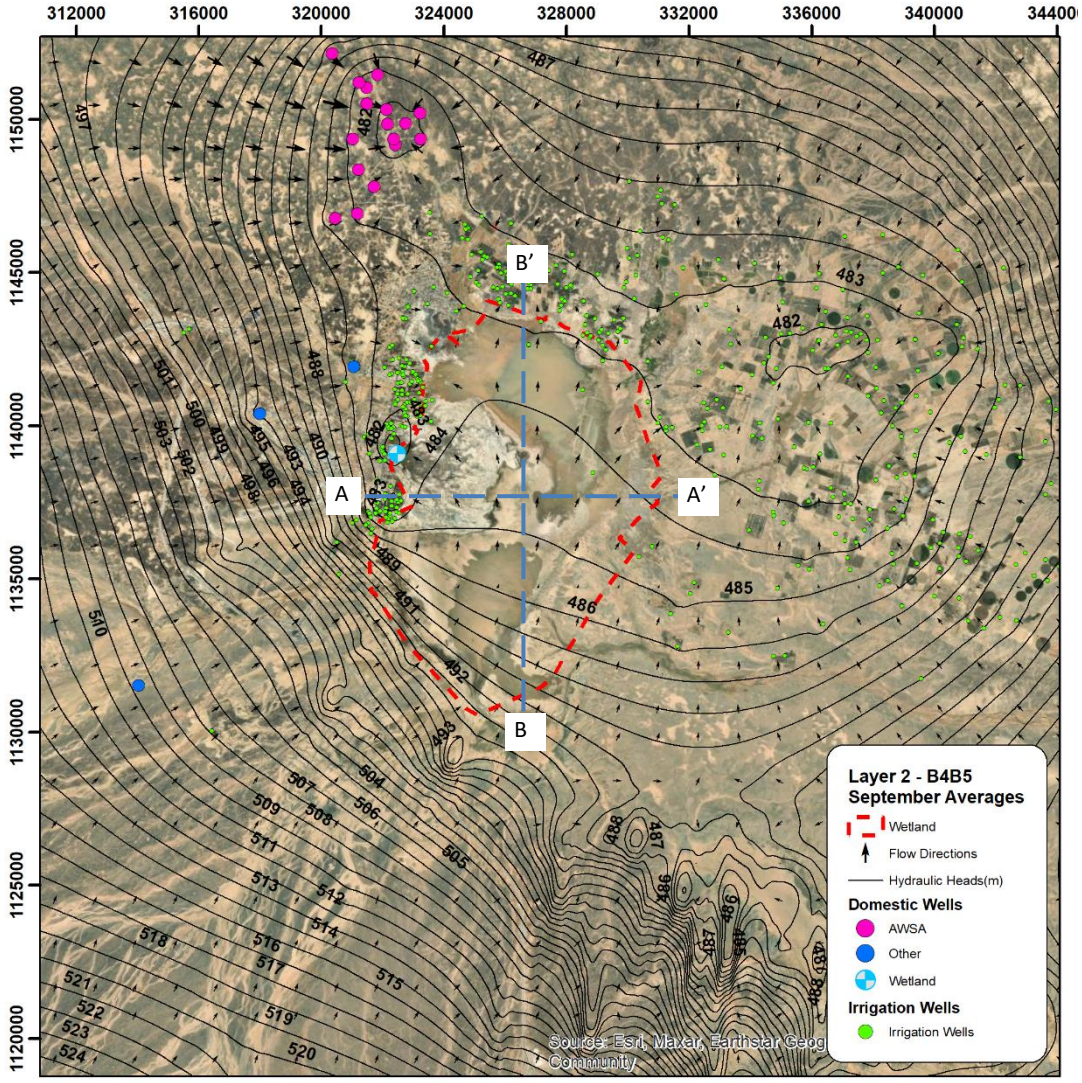

Figure 5-5. Temporally averaged hydraulic head distribution in Layer 2 calculated from model solutions of the month of September.

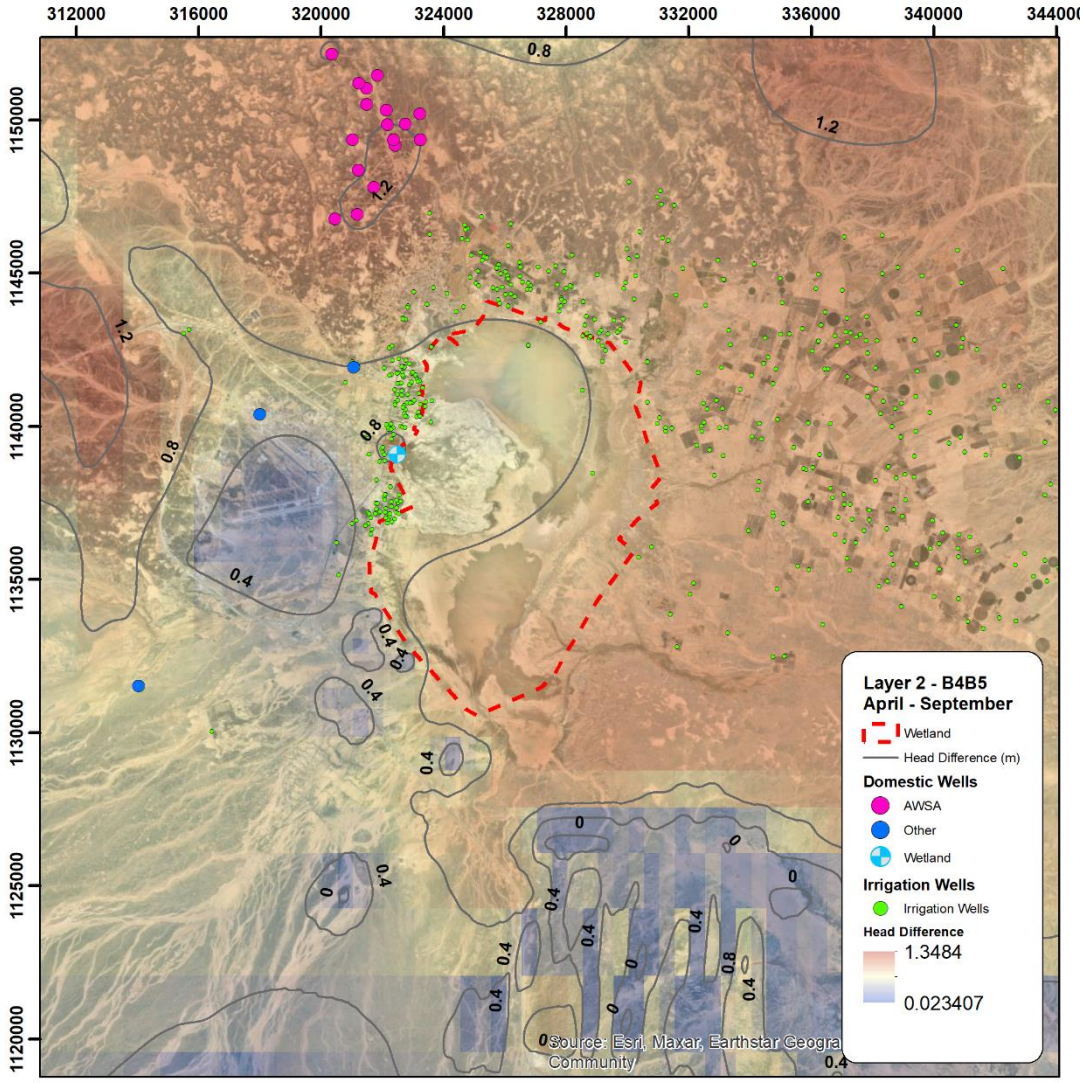

Figure 5-6. Seasonal difference in groundwater levels in and around the AWR. Red colors show larger differences.

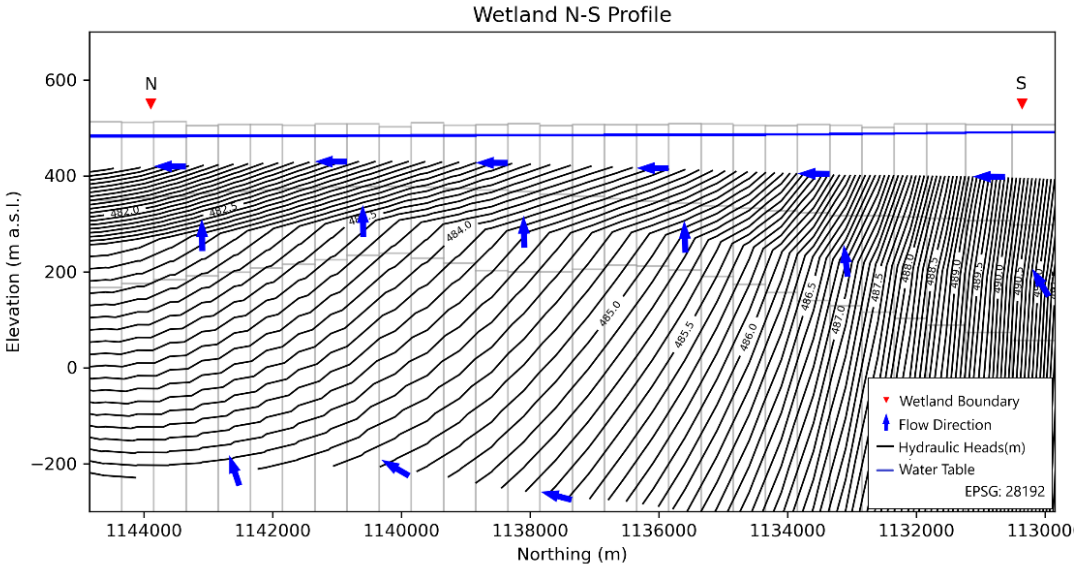

Figure 5-7. Simulated groundwater flow along cross-section B-B'.

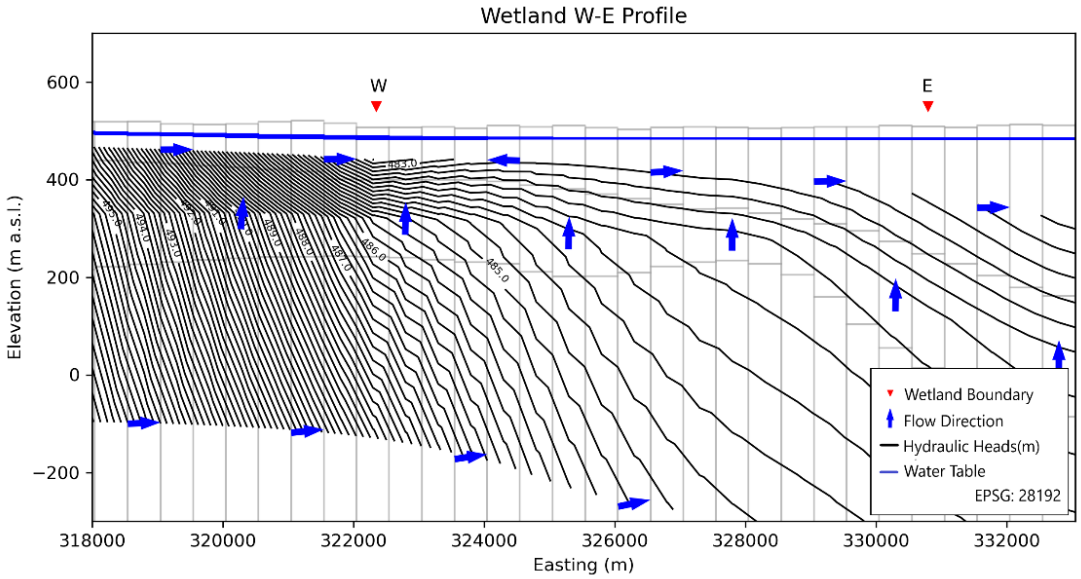

Figure 5-8. Simulated groundwater flow along cross-section A-A'.

Simulated hydrographs of the water table in the center of the AWR are presented in Figure 5-9. According to simulation results, the level of the water table has been declining from 490.4 m to 483.5 m over the 8-year modeling period. Although groundwater has periodically recovered in every rainy season by 0.5 – 1 m, the trend in the decline of levels has remained unchanged. It can be concluded that based on the model results, groundwater levels in the AWR decrease at an average rate of 0.86 m per year.

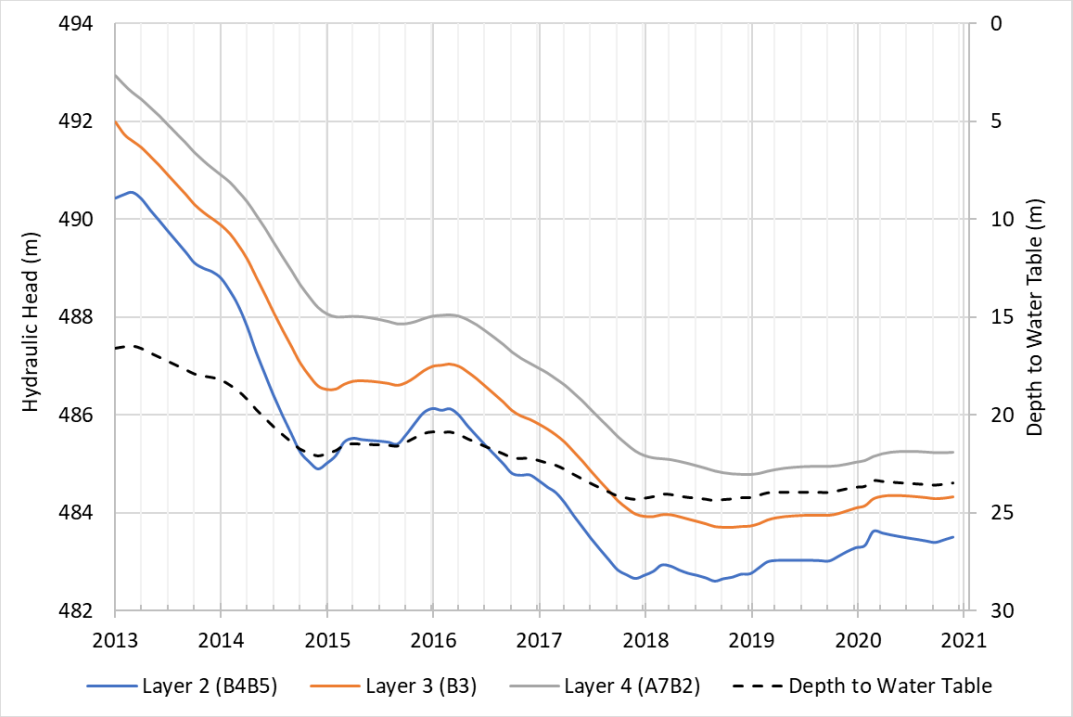

Figure 5-9.Temporal change in hydraulic heads and water table depth inside the AWR.

5.3 Simulated Groundwater Budgets

The simulated groundwater budget characterizes inflows and outflows to the Azraq Basin aquifer system and includes groundwater exchange with the saturated zone pore volume storage. Mean annual groundwater budgets were calculated (Figure 5-10), and the transient groundwater budgets were summarized for each month of the January 2013 – December 2020 simulation period (Figure 5-11).

The inflow components of the simulated groundwater budget consisted of infiltration from precipitation, and contribution from aquifer storage. Groundwater discharge occurred by pumping wells, evapotranspiration, and storage in the aquifer. For the entire simulation period it can be concluded that on an annual average basis, 43% of the inflow came from infiltration (90.14 Mm^3/yr). The remaining 57% is replenishment from storage (119.62 Mm^3/yr). On the outflow side, most of the groundwater is transferred back to aquifer storage (62%), whereas 27% of the outflow (57.47 Mm^3/yr) is well discharge, and 11% of the outflow (22.78 Mm^3/yr) was lost by evapotranspiration. Consequently, the resulting net groundwater recharge from precipitation excluding the well discharge was estimated at R = 90.14 – 22.78 = 67.36 Mm^3/yr.

Groundwater budget simulation results based on monthly changes showed that inflow and outflow terms typically fluctuated seasonally and between years, corresponding mostly with variations in the precipitation regime during the 8-year simulation period (Figure 5-11). Noteworthy is that the seasonal difference in the magnitude of the budget components can be pronounced.

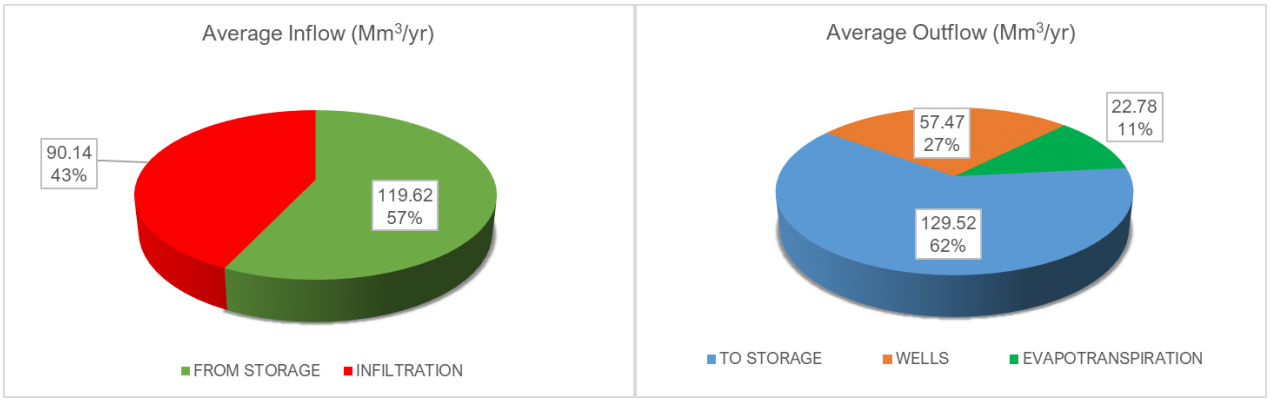

Figure 5-10. Simulated groundwater budget for the Jan 2013 - Dec 2020 simulation period expressed in mean yearly flow rates.

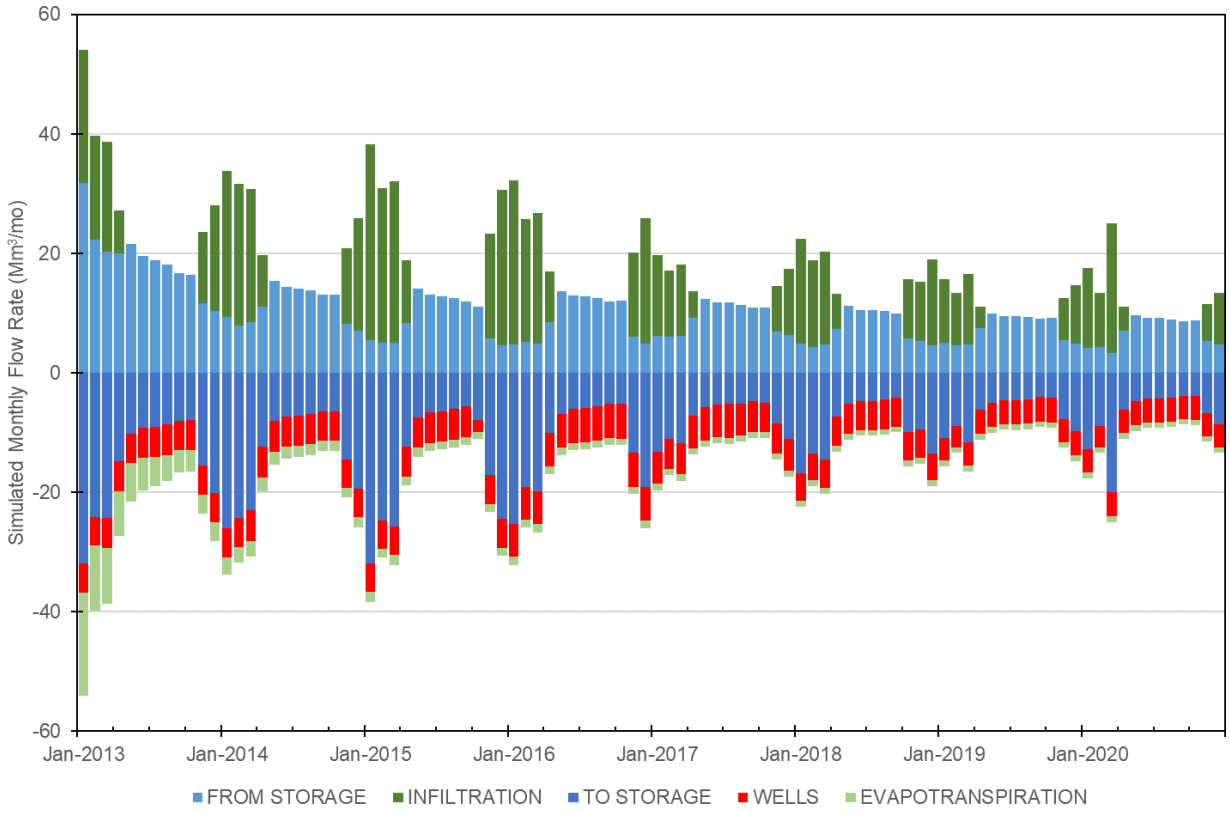

Figure 5-11. Simulated monthly flow budget time series.

6. SUMMARY AND CONCLUSIONS

This report presents the results of a modeling study conducted for the Azraq Basin with a focus on the groundwater flow patterns in and around the AWR. Previous modeling studies for the Azraq basin (Abdulla et al., 2000; Al-Kharabsheh, 2000; Abu-El-Sha'r and Hatemleh, 2007; Alkhatib, 2017) had different objectives, therefore the setup of boundary conditions, the extent of the model domain, temporal discretization, and conceptualization of hydrogeological layers differed among models. Therefore, a quantitative comparison of the results from previous studies is not considered to be meaningful. The modeling approach of the present study is simple with respect to boundary conditions but is rigorous in accounting for the variability of hydrological stresses.

The total discharge of groundwater through irrigation and public water supply wells was less than the net recharge. However, it should be noted that a significant amount of total groundwater discharge could probably not be accounted for in the model due to a lack of information about unlicensed wells in the Azraq Basin.

Modeling results provided critical information about the change in groundwater levels over the past 8 years. It can be concluded that the groundwater levels in the AWR are highly dependent on the groundwater flow and budget components in the basin as a whole. According to model results, the groundwater level in the AWR declines an average of 0.83 m per year.

The measures of model fit indicated that overall the model errors are acceptable. The flow simulation appropriately represents the regional patterns of groundwater flow in the Azraq Basin and yields meaningful water balances, comparable with results from previous estimation studies.

Regarding the model limitations, it should be noted that a groundwater flow model is a simplified approximation of actual conditions in the field. The accuracy and reliability of modeling results depend mostly on the accuracy/uncertainty of the input data. Therefore, the modeling process should be viewed as an iterative process where an effort to improve the model should be made if new information about the study site and the aquifer system is available. For a better interpretation of model results the following limitations of the flow model should be considered:

1) The temporal distribution of model calibration data is unbalanced such that head measurements are sporadic for the second half of the simulation period. Therefore, model results for the most recent period should be associated with relatively higher uncertainty.
2) The uncertainty in groundwater pumping input data is considered to be significant given that the database did not include information about unlicensed wells.
3) Optimized parameter sets resulting from groundwater flow model calibration are often non-unique, i.e. more than one combination of parameters exists that can provide similar fits to calibration targets. To mitigate this problem, more calibration data in the form of other types such as hydraulic gradient measurements or flow measurements would be necessary.

REFERENCES

- Abdulla, F. A., Al-Khatib, M. A., & Al-Ghazzawi, Z. D., 2000. Development of groundwater modeling for the Azraq Basin, Jordan. Environmental Geology, 40(1), 11–18.
- Abu-El-Sha'r W., Hatamleh, R., 2007. Using Modflow and MT3D groundwater flow and transport models as a management tool for the Azraq groundwater system, Jordan. J Civil Eng 1(2):153–172.
- Al-Kharabsheh, A., 1995. "Possibilities of artificial groundwater recharge in the Azraq Basin: potential surface water utilization of five representative catchment areas (Jordan)". PhD Thesis, Selbstverlag des Lehr- u. Forschungsbereichs Hydrologie und Umwelt am Inst. für Geologie, Germany.
- Alkhatib, J., 2017. "An Integrated Approach of Analyzing Management Solutions for the Water Crisis in Azraq Basin, Jordan". Doctoral dissertation, Niedersächsische Staats- und Universitätsbibliothek Göttingen).
- Alkhatib, J., Engelhardt, I., Ribbe, L., & Sauter, M., 2019. An integrated approach for choosing suitable pumping strategies for a semi-arid region in Jordan using a groundwater model coupled with analytical hierarchy techniques. Hydrogeology Journal, 27(4), 1143–1157.
- Alraggad, M., & Jasem, H., 2010. Managed Aquifer Recharge (MAR) through Surface Infiltration in the Azraq Basin/Jordan. Journal of Water Resource and Protection, 2(12), 1057–1070.
- Ayed, R., 1996. Hydrological and hydrogeological study of the Azraq basin. Ph.D. Thesis. Univ Baghdad, Baghdad, Iraq, pp 85–96.
- Doherty, J., 2016. PEST, Model-independent parameter estimation—User manual parts I and II (6th ed.), Brisbane, Australia, Watermark Numerical Computing.
- El-Naqa, A., 2010. Final Report Study of saltwater intrusion in the Upper Aquifer in Azraq Basin. IUCN-International Union for Conservation of Nature.
- El-Naqa, A., 1994. Estimation of transmissivity from specific capacity data in fractured carbonate rock aquifer, central Jordan. Environ. Geol. 23, 73–80.
- GTZ and NRA, 1977. "National Water Master Plan of Jordan". Agrar-und Hydrotechnik GmBH, Bundesanstalt fur Geowissenschaften und Rohstoffe, Hannover, Germany.
- Harbaugh, A.W., 2005. MODFLOW-2005, the U.S. Geological Survey modular ground-water model-the Ground-Water Flow Process: U.S. Geological Survey Techniques and Methods 6-A16, variously paginated.
- Harbaugh, A.W., Langevin, C.D., Hughes, J.D., Niswonger, R.D., Konikow, L.F., 2019. MODFLOW-2005 version 1.12.00, the U.S. Geological Survey modular groundwater model: U.S. Geological Survey Software Release, 03 February 2017.
- Hill, M.C., Banta, E.R., Harbaugh, A.W., Anderman, E.R., 2000. MODFLOW-2000, the U.S. Geological Survey modular ground-water model; user guide to the observation, sensitivity, and parameter-estimation processes and three post-processing programs, Open-File Report. Denver, CO.
- Hobler, M., Margane, A., Almomani, M. & Subah, A., 2001. "Groundwater resources of northern Jordan, Volume-4 contribution to the hydrogeology of Northern Jordan". BGRWAJ technical cooperation project.
- Ibrahim, K. M., and El-Naqa, A. R., 2018. Inverse geochemical modeling of groundwater salinization in Azraq Basin, Jordan. Arabian Journal of Geosciences, 11(10), 1-15.

- Illani S, Harlavan Y, Tarawneh K, Rabba' I, Weinberger R, Ibrahim KM, Peltz S, Steinitz G., 2001. New K–Ar ages of basalts from the Harrat Ash Shaam volcanic field in Jordan: implications for the span and duration of the upper mantle upwelling beneath the western Arabian plate. Geology 29:171–174.
- IWMI, 2017. "Groundwater Governance in Jordan: The case of Azraq Basin". Policy White Paper, Groundwater Governance in the Arab World, International Water Management Institute.
- Margane, A., Hobler, M., Almomani, M., Subah, A., 2002. "Contributions to the hydrogeology of Northern and Central Jordan". Bundesanstalt fuer Geowissenschaften und Rohstoffe und den Staatlichen Geologischen Diensten in der Bundesrepublik Deutschland (Ed.), Geologisches Jahrbuch. Reihe C (Hydrogeologie, Ingenieurgeologie). Stuttgart, Schweizerbart.
- MWI and BGR (Ministry of Water and Irrigation; Bundesanstalt für Geowissenschaften und Rohstoffe), 2019. "Groundwater Resource Assessment of Jordan 2017", Amman, Jordan.
- Rimawi, O., 1985. "Hydrogeochemistry and isotope hydrology of the ground-and surface water in North Jordan (North-Northeast of Mafraq, Dhuleil-Hallabat, Azraq-Basin): Hydrogeochemie und Isotopenhydrologie der Grund-und Oberflächenwässer in Nord-Jordanien (nord-nordöstlich von Mafraq, Dhuleil-Hallabat, Azraq-Becken)". Ph.D. dissertation, TU München, Germany.
- Salameh, E., & Udluft, P., 1985. The hydrodynamic pattern of the central part of Jordan. Geologisches Jahrbuch, Reihe C, Hydrogeologie, Ingenieurgeologie, (38), 39-53.
- Winston, R.B., 2009, ModelMuse-A graphical user interface for MODFLOW-2005 and PHAST: U.S. Geological Survey Techniques and Methods 6-A29, 52 p.
- Winston, R.B., 2022, ModelMuse version 5.1.1: U.S. Geological Survey Software Release, 15 November 2022, https://doi.org/10.5066/P90QQ94D.